AD-A167 971 MOLECULAR DYNAMICS OF A MODEL SN2 REACTION IN WATER(U) 1/1
CALIFORNIA UNIV SAN DIEGO LA JOLLA DEPT OF CHEMISTRY
J P BERGSMA ET AL. 01 MAY 86 N00014-78-C-0325

UNCLASSIFIED F/G 7/4 NL

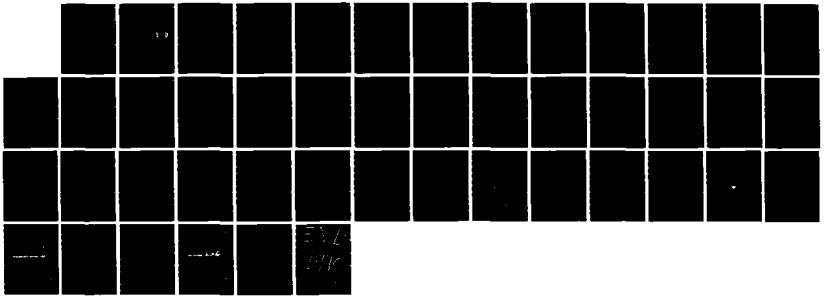

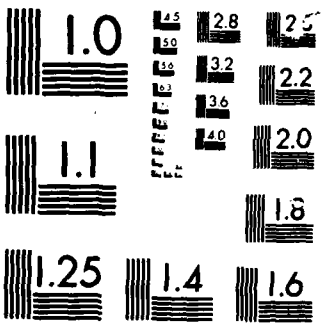

MICROCOPY CHART

(12)

OFFICE OF NAVAL RESEARCH

Contract N00014-78-C-0325

TECHNICAL REPORT

MOLECULAR DYNAMICS OF A MODEL S_N2 REACTION IN WATER

by

John P. Bergsma, Bradley J. Gertner, Kent R. Wilson*
James T. Hynes+

Prepared for Publication

in

Journal of Chemical Physics

* Department of Chemistry, University of California, San Diego, La Jolla, CA 92093
+ Department of Chemistry, University of Colorado, Boulder, CO 80309

May 1, 1986

SECURITY CLASSIFICATION OF THIS PAGE (When Data Entered)

REPORT DOCUMENTATION PAGE		READ INSTRUCTIONS BEFORE COMPLETING FORM
1. REPORT NUMBER N00014-78-C-0325	2. GOVT ACCESSION NO.	3. RECIPIENT'S CATALOG NUMBER
4. TITLE (and Subtitle) Molecular Dynamics of a Model S_N2 Reaction in Water		5. TYPE OF REPORT & PERIOD COVERED Technical Report 6. PERFORMING ORG. REPORT NUMBER
7. AUTHOR(s) John P. Bergsma, Bradley J. Gertner, Kent R. Wilson James T. Hynes		8. CONTRACT OR GRANT NUMBER(s) N00014-78-C-0325
9. PERFORMING ORGANIZATION NAME AND ADDRESS THE REGENTS OF THE UNIVERSITY OF CALIFORNIA University of California, San Diego La Jolla, California 92093		10. PROGRAM ELEMENT, PROJECT, TASK AREA & WORK UNIT NUMBERS
11. CONTROLLING OFFICE NAME AND ADDRESS Office of Naval Research 800 North Quincy Street Arlington, Virginia 22217		12. REPORT DATE May 1, 1986 13. NUMBER OF PAGES 43
14. MONITORING AGENCY NAME & ADDRESS(if different from Controlling Office) Office of Naval Research Resident Representative Mail Code A-043 University of California, San Diego La Jolla, California 92093		15. SECURITY CLASS. (of this report) Unclassified 15a. DECLASSIFICATION/DOWNGRADING SCHEDULE

16. DISTRIBUTION STATEMENT (of this Report)

Approved for public release; distribution unlimited.

17. DISTRIBUTION STATEMENT (of the abstract entered in Block 20, if different from Report)

18. SUPPLEMENTARY NOTES

The views, opinions, and/or findings contained in this report are those of the author(s), and should not be construed as an official Department of the Navy position, policy, or decision, unless so designated by other documentation.

19. KEY WORDS (Continue on reverse side if necessary and identify by block number)

20. ABSTRACT (Continue on reverse side if necessary and identify by block number)

Molecular dynamics are computed for a model S_N2 reaction $Cl^- + CH_3Cl \rightarrow ClCH_3 + Cl^-$ in water and are found to be strongly dependent on the instantaneous local configuration of the solvent at the transition state barrier. There are significant deviations from the simple picture of passage over a free energy barrier in the reaction coordinate, and thus, a marked departure from Transition State Theory occurs in the form of barrier recrossings. Factors controlling the dynamics are discussed, and in particular, the rate of change of atomic charge distribution along the

(OVER)

DD FORM 1 JAN 73 1473 EDITION OF 1 NOV 65 IS OBSOLETE

SECURITY CLASSIFICATION OF THIS PAGE (When Data Entered)

MOLECULAR DYNAMICS OF A MODEL S_N2 REACTION IN WATER

John P. Bergsma, Bradley J. Gertner, Kent R. Wilson

Department of Chemistry
University of California, San Diego
La Jolla, CA 92093

James T. Hynes

Department of Chemistry
University of Colorado
Boulder, CO 80309

ABSTRACT

Molecular dynamics are computed for a model S_N2 reaction $Cl^- + CH_3Cl \rightarrow ClCH_3 + Cl^-$ in water and are found to be strongly dependent on the instantaneous local configuration of the solvent at the transition state barrier. There are significant deviations from the simple picture of passage over a free energy barrier in the reaction coordinate, and thus, a marked departure from Transition State Theory occurs in the form of barrier recrossings. Factors controlling the dynamics are discussed, and, in particular, the rate of change of atomic charge distribution along the reaction coordinate is found to have a major effect on the dynamics. A simple frozen solvent theory involving nonadiabatic solvation is presented which can predict the outcome of a particular reaction trajectory by considering only the interaction with the solvent of the reaction system at the gas-phase transition barrier. The frozen solvent theory predicts the adjustment (the transmission coefficient κ) needed to make the transition state theory rate agree with the outcome of the molecular dynamics trajectories.

Submitted to J. Chem. Phys.

MOLECULAR DYNAMICS OF A MODEL S_N2 REACTION IN WATER

John P. Bergsma, Bradley J. Gertner, Kent R. Wilson

Department of Chemistry
University of California, San Diego
La Jolla, CA 92093

James T. Hynes

Department of Chemistry
University of Colorado
Boulder, CO 80309

I. Introduction

The bimolecular nucleophilic substitution S_N2 reaction, $X^- + RY \rightarrow RX + Y^-$, is one of the most fundamental of organic reactions. It has been extensively studied in solution, and these studies are a source of many basic ideas in physical-organic chemistry; examples include nucleophilicity, leaving-group ability and solvent effects.[1-3] This reaction is well known to be experimentally sensitive to solvent polarity,[1-4] and, beginning with the famous work of Hughes and Ingold,[5-7] solvent effects have been interpreted in terms of the equilibrium solvation thermodynamic free energies of activation of the transition state complex. This theme has been pursued in modern statistical mechanics in a Monte Carlo equilibrium simulation of $Cl^- + CH_3Cl$ by Jorgensen and coworkers[8,9] and in integral equation work by Chiles and Rossky.[10] In this paper we use the Molecular Dynamics simulation technique to explore a quite different and novel aspect of the reaction pathway: The role of polar-solvent dynamics and configurations in affecting, at the molecular level, the reaction trajectories and the value of the rate constant.

These last ingredients have been explored for general charge transfer reactions in analytic model studies by van der Zwan and Hynes.[11-13] These studies point strongly to the importance of nonequilibrium solvation effects on charge transfer rates in polar solvents. The present work examines these questions for a more realistic reaction in a realistic solvent.

Our method is simple and direct and follows along the general lines of our previous investigations[14,15] of the A + BC reaction in rare gas solvent. We use molecular dynamics computational simulation to examine model S_N2 reactions roughly patterned after the $Cl^- + CH_3Cl$ reaction in water. The intrinsic S_N2 potential is taken to be the form of a double well, established in gas phase experiments[2,3,16] and quantum mechanical calculations,[8,17-20] but we take the methyl group as simplified to a single united atom. A fairly realistic model for flexible water is adopted.[21]

We find that, even for high, sharp central barriers, the ability of the solvent to influence the trajectories of the reacting atoms, and thus to lower the rate constant from the simple Transition State Theory prediction, is significant. The molecular level picture of the reaction dynamics differs considerably from that painted by an equilibrium free energy picture in which equilibrium solvation is assumed. We find that the transition state is characterized by nonequilibrium, nonadiabatic solvation;[11-13] the solvent is effectively "frozen" and cannot adjust rapidly enough on the relevant time scales to provide equilibrium solvation. We explore this reaction as a function of reaction barrier height and curvature, characteristics of charge redistribution along the reaction coordinate, and factors controlling solvent molecule reorientation time.

The outline of this paper is as follows. In Sec. II we describe the methodology, selection of the potential energy surfaces and the prescription for the charge redistribution rate along the reaction coordinate. In Sec. III we analyze the reaction results for a barrier height similar to that of the actual $Cl^- + CH_3Cl$ reaction, while Sec. IV explores the consequences of different barrier heights and curvatures, variation of charge switching rate and modification of the water hydrogen mass. Section V is the conclusion and summary. Certain details of the calculation are relegated to the Appendices. A companion paper[22] describes in more detail an analytic model to describe our results.

II. Methodology and Potentials

A. Molecular Dynamics

Molecular dynamics is used to compute time histories of the position and momentum coordinates for all of the atoms in a system subject to truncated octahedral[23] periodic boundary conditions. This is accomplished by numerical integration of Hamilton's equations of motion for classical particles

$$\dot{\mathbf{r}}^N = \frac{\partial H}{\partial \mathbf{p}^N} , \tag{2.1}$$

and

$$\dot{\mathbf{p}}^N = - \frac{\partial H}{\partial \mathbf{r}^N} , \tag{2.2}$$

in which $\mathbf{p}^N$ and $\mathbf{r}^N$ are the conjugate momentum and position variables for a system containing N unique particles, and H is the full Hamiltonian for the system.

A modified Verlet algorithm,[24-26] incorporating a time step of 0.5 femtoseconds, is used to integrate these equations of motion. There are 64 water molecules used in most of the liquid simulations, and 263 water molecules in a limited set of test calculations.

These calculations are carried out on a Floating Point Systems AP120B array processor attached to a VAX 11/780 host computer. For 64 water solvent molecules and the reacting solute, 1000 time steps require 300 seconds of real time on the array processor. The calculations presented in this paper required 80 days of array processor time, and would have required 7.5 years of dedicated VAX 11/780 time without the array processor.

B. Potentials

The potential energy surface used in the Hamiltonian in Eqs. (2.1) and (2.2) is intended to be a simplified representation of the model S_N2 reaction, $Cl^- + CH_3Cl \rightarrow ClCH_3 + Cl^-$, occurring in liquid water solvent. The total potential is composed of the potentials representing smaller parts of the problem as described below.

1. S_N2 Gas Phase Potential

Our S_N2 gas phase potential is very roughly modeled after the one-dimensional $Cl^- + CH_3Cl \rightarrow CH_3Cl + Cl^-$ *ab initio* gas phase potential of Jorgensen and co-workers.[8,9] The Jorgensen potential was only given along a reaction coordinate defined as the gas phase minimum potential energy path between reactants and products. To describe a full three-dimensional potential energy surface for our model S_N2 reaction we use a London-Eyring-Polanyi-Sato (LEPS)[27] potential energy function. This incorporates the main features of the one-dimensional, double-well potential determined by Jorgensen, including the calculated barrier height, but uses a united atom representation for the central CH_3 group. The form of the LEPS potential is

$$\Phi^{LEPS}(r_1,r_2,r_3) = Q_1 + Q_2 + Q_3 - (J_1^2 + J_2^2 + J_3^2 - J_1J_2 - J_2J_3 - J_3J_1)^{1/2} , \tag{2.3}$$

in which r_1 and r_2 are the variable bond lengths between the CH_3 united atom and the two Cl atoms, r_3 is the bond length between the two Cl atoms, and Q_i and J_i are linear combinations of the "singlet" and "triplet" diatomic energies:

$$Q_i(r_i) = ({}^1E_i + {}^3E_i)/2 , \tag{2.4}$$

and

$$J_i(r_i) = ({}^1E_i - {}^3E_i)/2 \,. \tag{2.5}$$

Here, the "singlet" ground state energy is represented as a Morse potential,

$${}^1E_i(r_i) = {}^1D_i\left\{1 - \exp\left[-{}^1\beta_i(r_i - {}^1r_i^0)\right]\right\}^2 - {}^1D_i \,, \tag{2.6}$$

while the "triplet" diatomic energy is an "anti-Morse" potential,

$${}^3E_i(r_i) = {}^3D_i\left\{1 + \exp\left[-{}^3\beta_i(r_i - {}^3r_i^0)\right]\right\}^2 - {}^3D_i \,. \tag{2.7}$$

The LEPS potential reduces to the diatomic bound Morse potential for an infinitely separated atom and diatomic (*i.e.* CH_3—Cl) and is highly adaptable, containing 18 non-symmetry adapted parameters (${}^1D_i$, ${}^3D_i$, ${}^1\beta_i$, ${}^3\beta_i$, ${}^1r_i^0$, ${}^3r_i^0$, for i = 1,2,3) which allow the simultaneous adjustment of barrier height and barrier frequency, ω_b, defined as the absolute value of the imaginary frequency of an inverted parabolic approximation to the potential at the saddle point along the minimum energy pathway from reactants to products, *i.e.* the reaction coordinate. We report all frequencies in spectroscopic wavenumber units, *i.e.* $(\omega_b/2\pi c)$ cm^{-1}, to facilitate comparison with spectroscopic vibrational properties. Table 1 shows the values of the 18 LEPS parameters used in the simulation of our model S_N2 reaction and variations which incorporate the basic features of the double-well potential employed by Jorgensen[8] and the isolated Morse potential fitted to the equilibrium value[28] of the normal mode asymmetric stretch vibrational frequency, 732.8 cm^{-1}, of CH_3—Cl. (Note that the LEPS potential *per se* allows bonding between the two chlorine atoms. We choose the Cl–Cl parameters to be free variables for fitting our potential to Jorgensen's potential, so they do not represent physical parameters.) Figure 1 illustrates potential energy contours for the 13.9 kcal/mol barrier in which the axes are skewed 44.4° from perpendicular to define a coordinate system which diagonalizes the kinetic energy matrix for this system.[27,29] (This allows classical dynamics to be represented by a single point mass sliding on the potential energy surface.) The key features of this potential are two wells characterizing ion-molecule complexes separated by a high transition barrier. Most of our calculations are performed on this three dimensional LEPS potential, which has a barrier of 13.9 kcal/mol with respect to the bottom of the ion-dipole complex wells and 3.6 kcal/mol with respect to separated $ClCH_3 + Cl^-$.

2. Solvent Potential

We adopt the semiempirical flexible water intermolecular potential of Watts[21] combined with the spectroscopic intramolecular water potential of Kuchitsu and Morino.[21,30] These water potentials have been used in molecular dynamics simulations to calculate thermodynamic quantities, energy, free energy and constant volume heat capacity, and vibrational normal mode frequencies [31,32] in good agreement with experiment after a quantum correction is added. In addition, the rotational time correlation functions and radial distribution functions of these waters compare favorably with other water models.[33]

3. Solvent-Solute Potential

Charges on the reaction system interact with charges on water molecules through coulomb potentials. The dipole moment on water (~1.86 D) is set by assigning partial charges of -0.66 electrons to oxygen atoms and +0.33 electrons to hydrogen atoms.[21] Because the waters are internally flexible, the dipole moment can fluctuate with changing internal nuclear coordinates. The partial charges on the three atoms in our model S_N2 reaction system sum to give the overall negative charge of one electron. The distribution of this charge along the reaction coordinate varies smoothly from reactants where the net charge is on the attacking chloride ion, to the transition barrier where it is shared equally between the two chlorine atoms, to the products where it is localized on the leaving chloride. Figure 2 illustrates the distribution of the partial charges on the three atoms as a function of a conveniently defined (for computational purposes) reaction measure, $r_{AB}^2 - r_{BC}^2$, in which r_{AB} is the distance between one Cl—CH_3 atom pair and r_{BC} is the distance between the other CH_3—Cl atom pair. This variation is largely modeled after the work of Jorgensen,[8] but with some modifications of the charge switching parameters

Table 1. $[Cl—CH_3—Cl]^-$ LEPS Potential Parameters			
Barrier Height (with respect to the bottom of the well, kcal/mol)	31.9	13.9	4.9
Barrier Frequency (magnitude, cm^{-1})	894	461	232
${}^1r_i^0$ (Å) i = 1,2	1.776382	1.776382	1.776382
${}^1r_3^0$ (Å)	2.094857	2.094857	2.094857
${}^3r_i^0$ (Å) i = 1,2	1.789255	1.785014	1.795583
${}^3r_3^0$ (Å)	2.135243	2.186060	2.175774
${}^1\beta_i$ ($Å^{-1}$) i = 1,2	0.934381	0.929968	0.936038
${}^1\beta_3$ ($Å^{-1}$)	0.639340	0.432955	0.705479
${}^3\beta_i$ ($Å^{-1}$) i = 1,2	4.512772	4.822681	4.853273
${}^3\beta_3$ ($Å^{-1}$)	1.048338	1.016811	1.036805
${}^1D_i$ (kcal/mol) i = 1,2	233.134491	234.524674	232.308932
${}^1D_3$ (kcal/mol)	308.573800	64.925971	-88.274115
${}^3D_i$ (kcal/mol) i = 1,2	261.994490	220.244820	261.021681
${}^3D_3$ (kcal/mol)	274.953525	284.999867	274.257166

for the central united atom (*cf* Appendix A). This shifting charge on the solute interacts with the surrounding solvent molecules through Coulombic potentials, with the partial charge on each solvent atom fixed.

A moving charge in the reacting system has an interesting effect on the forces between the solute and solvent atoms. The three atoms in the reacting system will "feel" a force from the solvent related to the switching charge which varies along the reaction coordinate in addition to the normal Coulombic force for fixed charges. Near the transition barrier the charge is shifting rapidly between the attacking and leaving chloride ions, and the extra force which arises is proportional to the rate of change of this charge distribution with respect to the reaction coordinate. At any instant only the reaction system feels this force, while all solvent molecules are unaffected by this extra charge switching force; the total force between the solute and solvent molecules is nevertheless conservative. This force is a "heavy particle polarization force", since displacement in the reaction coordinate shifts the electronic distribution instantaneously (in the electronic adiabatic limit). We will find that this shifting charge force has important consequences in the dynamics of the S_N2 reaction.

The van der Waals forces between solute and solvent atoms are described using simple Lennard-Jones 6-12 potentials. If required, the Lennard-Jones parameters for the solute could be made to vary with reaction coordinate[8] in a similar manner to the charge variation, but we choose to keep them constant. Mathematical details of the solvent-solute potential and forces are given in Appendix A.

The computed Cl-H and Cl-O radial distribution functions (rdf's) of the reactants at the transition barrier with the water solvent compare well to the rdf's of Jorgensen.[9] In addition, the pair interaction distribution functions for a single chloride ion in water, computed with the pure water potential (see above) and with the Lennard-Jones and Coulombic parameters for chlorine-water interactions, compare well with the pair-interaction energies determined by Vogel and Heinzinger for lithium chloride and

cesium chloride in water.[34,35]

4. Switching Functions

In simulating this S_N2 reaction, $Cl^- + CH_3Cl \rightarrow ClCH_3 + Cl^-$ in a polar solvent, special care must be taken in "feathering", *i.e.* smoothly ramping, the potentials properly to zero by the edge of the boundary conditions to avoid force discontinuities and nonphysical buildup of net charges on molecules. To accomplish this we define certain switching regions wherein the forces are damped near the edge of our periodic boundary conditions on a molecule-by-molecule basis. The interactions among solvent molecules and of the solvent molecules with the charged reactant species are computed for each molecule-molecule pair. The distance between a particular molecule-molecule pair is defined as the distance between one molecule and the nearest periodic image of the other molecule[23] (*cf* Appendix B). Forces calculated between these two imaged molecules are damped when this distance becomes close to the periodic boundary length, and are zero when this distance is equal to the periodic boundary length.

A difficulty in simulating the motion of the solute atoms along the reaction coordinate lies in maintaining the overall neutrality of the methyl chloride species away from the transition barrier. On the reactant side, ($Cl^- + CH_3Cl$), the CH_3Cl is imaged with all other molecules as a single molecule because it has a non-zero dipole moment. Similarly, on the product side ($ClCH_3 + Cl^-$), the $ClCH_3$ is imaged as one molecule. Although imaging the entire $[Cl—CH_3—Cl]^-$ complex is possible, the short range interactions with either the ion or the molecule would be underestimated due to the damping by the switching function at large distances. To solve this problem the ion and the molecule are imaged separately by switching the definition of the grouping from reactant to products on either side of the transition barrier in a continuous manner. This is explained in detail in Appendix B.

C. Initial Conditions

The molecular dynamics of activated barrier crossing are computed using a technique due to Keck[36] and Anderson,[37] (see also Bennett[38]) in which trajectories are initialized from an equilibrium distribution at the top of the energy barrier, and dynamics are computed both forward and backward in time from the initial conditions. This general method has been applied to the study of defect motion,[39] isomerization dynamics,[40] protein dynamics,[41-43] and surface desorption,[44] as well as to the dynamics of the A + BC reaction in rare gas solvents.[14,15]

We use molecular dynamics to compute an ensemble of trajectories initially selected at the transition barrier but, as described below, originating and ending with reactants or products and analyze the results by examining statistical and average properties of the ensemble. Examples of these are the number of barrier recrossings and the details of the energy exchange with the solvent.

The average value of some quantity, $\langle A \rangle$, in a classical ensemble is

$$\langle A \rangle = \frac{\iint d\mathbf{r}^N d\mathbf{p}^N \, A \, e^{-H(\mathbf{r}^N,\mathbf{p}^N)/k_BT}}{\iint d\mathbf{r}^N d\mathbf{p}^N \, e^{-H(\mathbf{r}^N,\mathbf{p}^N)/k_BT}} , \tag{2.8}$$

where $\mathbf{r}^N$ is a vector of the N Cartesian coordinates of the system, $\mathbf{p}^N$ is a vector of the momentum coordinates conjugate to $\mathbf{r}^N$, $H(\mathbf{r}^N,\mathbf{p}^N)$ is the full Hamiltonian of the system, k_B is Boltzmann's constant and T is the temperature. The initial conditions $\mathbf{r}^N$ and $\mathbf{p}^N$ are selected from a Boltzmann distribution on the transition barrier which, in the gas phase (and for very weak solvent-solute interactions), can be conveniently defined as lying on the symmetric stretch and bend coordinates of $[Cl—CH_3—Cl]^-$ through the lowest lying saddle point on the gas phase LEPS potential surface. The reaction coordinate is defined to be the asymmetric stretch, and the absolute value of the normal mode imaginary frequency associated with the asymmetric stretch coordinate on the gas phase potential surface is defined as the barrier frequency, ω_b. Although we describe in a previous paper[15] a method for evaluating Eq. (2.8) under conditions of weak solvent-solute interactions, that method is not applicable here since there are very strong charge-charge interactions between the solute and water solvent.

To describe our current procedure, we first note that the reaction is symmetric with respect to reactants and products. This implies that the average value of the asymmetric stretch coordinate is zero. Thus, if there is a single saddle point, the average location of the transition barrier must correspond to

zero asymmetric stretch and lie somewhere along the symmetric stretch and bend coordinates of $[Cl—CH_3—Cl]^-$. The potential energy surface on which we choose initial conditions for the solute must include, in addition to the gas phase potential, the effect of the strong intermolecular potential energy of interaction with the solvent. Therefore, our initial conditions are chosen by first constraining the asymmetric stretch position and momentum of $[Cl—CH_3—Cl]^-$ to be zero while molecular dynamics selects values of all the other degrees of freedom in the system. This constraint is performed by forcing, at each time step, the lengths of the two $CH_3—Cl$ bonds to be equal, and removing all momenta and force along the asymmetric stretch. After a 2.0 ps equilibration period to allow the other degrees of freedom to randomize, the asymmetric stretch momentum is initialized from a Boltzmann distribution at temperature 298 K, the constraint on the reaction coordinate is released, and dynamics are computed both forward and backward in time long enough to observe on both ends of the trajectory whether a stable product or reactant is formed. It is important to note that, in contrast to our earlier A + BC in rare gas solvent studies[14,15] where we used quadrature techniques which gave each trajectory a different weighting in the ensemble, in this paper we let the dynamics randomly choose the initial conditions so that all of the trajectories have equal weighting in the ensemble average.

To investigate the possibility that the solvent might be "trapped" in a local solvent potential minimum (and thus that a similar solvent configuration might persist between trajectory runs), a series of tests was made in which the entire $[Cl—CH_3—Cl]^-$ molecule is held fixed while the solvent is heated to a temperature of 5000 K, the molecular dynamics run for 1.0 ps of simulation time in order to expel the solvent out of any local minima, and the solvent then cooled back down to 298 K. The high temperature equilibration is found to give results similar to those obtained with 298 K equilibration, and the majority of our runs are thus made with equilibration at 298 K.

III. Results for Model $Cl^- + CH_3Cl$ Reaction

In this section we present the results for the model S_N2 reaction of $Cl^- + CH_3Cl$ in both gas phase and in liquid water. There are 64 water molecules in the simulation of the liquid at a density of 1.0 g cm^{-3}. Using a larger system is desirable, but this would make the calculations impractically time-consuming since the amount of computer time required to simulate the dynamics is considerable, even for the small solvent system of 64 waters. Thus, a small subset of the dynamics is computed for a larger system containing 263 solvent water molecules to check that there are no significant differences between the dynamics obtained for the smaller and larger systems. Molecular dynamics calculations with the larger 263 water system take approximately 16 times longer than with the smaller system, so it is possible to generate only 6 trajectories (with a total simulated time of 15 ps) per day, even with the use of the array processor.

A. Gas Phase Dynamics

Although our focus is on reaction dynamics in solution, the dynamics in the gas-phase[2,45] is of sufficient interest to warrant a brief exposition. Figure 1 shows an energy contour plot of the gas-phase potential energy surface in which the double well character centered about the asymmetric stretch reaction coordinate in the transition barrier region can be clearly seen. The central transition energy barrier is higher in energy than the asymptotic potential energy of the separated Cl^- ion and CH_3Cl by 3.6 kcal/mol, so there is sufficient energy for a trajectory starting at the transition barrier to escape from the low energy product well past the transition barrier and form separated products. However, this is *not* what is observed; instead the trajectories are *trapped* in the ion-dipole complex energy well for a time measuring much longer than our standard simulation time of ± 0.5 ps. A vibrationally "hot" complex is formed which oscillates inside the well for some time before breaking up. In addition, there are some *recrossings* of the transition barrier as the complex passes from the product well to the reactant well. Table 2 shows crossing patterns for 128 trajectories, each of which is integrated out to time 0.5 ps before and after the transition barrier. Here, "products" are defined as the $ClCH_3—Cl^-$ ion-molecule complex. Trajectories always begin with initially forward momentum toward products along the asymmetric stretch reaction coordinate, and Table 2 indicates that 107 out of 128 trajectories became "products" on the ± 0.5 ps time scale on which we followed the dynamics. However, very few of these trajectories actually escaped the wells, but instead formed a metastable complex. The other 21 trajectories actually recossed the transition barrier at least once and then remained localized in the appropriate

Table 2. 13.9 kcal/mol Barrier Crossings for $Cl^- + CH_3Cl$ in Gas Phase				
Number of Crossings	Initial and Final States of Trajectories			
	Reactant - Reactant	Reactant - Product	Product - Reactant	Product - Product
1	0	107	0	0
2	10	0	0	9
3	0	0	2	0

complex well.

One interesting way to examine the features of isolated-complex dynamics is to monitor the redistribution of internal energy in the reaction system as a function of time. One way to partition the total energy is into $[Cl—CH_3—Cl]^-$ potential energy, $[Cl—CH_3—Cl]^-$ potential energy plus $CH_3—Cl$ vibrational kinetic energy, $CH_3—Cl$ rotational and translational kinetic energy, and the translational kinetic energy of Cl^-. Figure 3 shows average energy partitioning patterns as a function of time for 128 trajectories in the gas phase. The vibrational kinetic energy plus total $[Cl—CH_3—Cl]^-$ potential energy is seen to increase to a maximum in about 0.25 ps before and after the transition barrier but decreases at longer times. This build up in energy and subsequent decrease is observed on a shorter time scale for the translational and rotational degrees of freedom. The kinetic energy at longer times is seen to transform into potential energy, and a metastable complex is formed. Complex formation is a result of the strong charge-dipole interaction close to the transition barrier and is characterized by the double-well feature of the potential surface. Even though there is total energy in excess of that required to escape to separated products from the bottom of the ion-dipole well, there clearly are coupled non-reactive degrees of freedom in the system into which the energy is redistributed on the time scale of our calculation. (Note that the methyl umbrella vibration is not a dynamical variable here.)

While the isolated-complex dynamics is an interesting subject for future research with implications for RRKM theory, we present it here solely to contrast with the reaction in solution. The following section examines the dynamics of this reaction system in water solvent.

B. Dynamics in Aqueous Solution

In the standard view[5,6] of solvent effects on the rates of S_N2 reactions, the solvent is assumed[11-13] to be in equilibrium at each stage of the "intrinsic" $X^- + RY$ reaction coordinate. In fact, it is assumed that the reaction coordinate depends only on the $X^- + RY$ system, and the polar solvent only modifies the gas-phase free energy profile along the reaction coordinate by lowering the free energy of the higher-charge-density reactants $X^- + RY$ and products $RX + Y^-$ more than the free energy of the dispersed-charge-density transition state $X^{\delta-}—R^{\delta+}—Y^{\delta-}$. Thus, the free energy of activation increases in solution relative to the gas phase,and the deep wells on either side of the transition barrier diminish considerably.[2,3,8,9] This is illustrated in Fig. 4, which shows a schematic representation of the free energy profile along the reaction coordinate for a symmetric S_N2 reaction of the form $X^- + RY$ in both the gas phase (solid line) and in a polar solvent (dashed line).[2,3,5,6] These features are borne out in explicit statistical mechanical calculations of reaction free energies.[8-10]

The free energy picture is a restricted view which makes no allowances for possible dynamical or non-equilibrium effects of solvent molecules on the details, or even the *fate* of individual reaction trajectories. Does the equilibrium picture for the solvent hold at all points along the reaction coordinate, and does the reaction always proceed to formation of products upon reaching the transition barrier with positive flux? Equivalently, are there nonequilibrium solvation effects[11-13] which lead to recrossing of the TST surface? The answers to these questions are critical in understanding S_N2 reaction dynamics in solution.

1. Barrier Recrossings

Each trajectory has initially positive momentum in the asymmetric stretch reaction coordinate which sends it toward products $ClCH_3 + Cl^-$. We have examined 400 solution phase trajectories with with a solvent composed of 64 water molecules. We find that the "no recrossing" assumption is often violated; further, the reaction fate is typically decided within the very short time period of 0.02 ps. The 13.9 kcal/mol energy barrier crossing patterns are presented in Table 3 and show that trajectories in solution exhibit predominantly 1 or 2 crossings.

Table 3. 13.9 kcal/mol Barrier Crossings for $Cl^- + CH_3Cl$ in Water

Number of Crossings	Initial and Final States of Trajectories			
	Reactant - Reactant	Reactant - Product	Product - Reactant	Product - Product
1	0	148	0	0
2	130	0	0	110
3	0	4	6	0
4	0	0	0	2

Of the 63% of trajectories which cross the barrier more than once, most recross only a single time. There is also a very small fraction of trajectories which have 3 or 4 crossings of the energy barrier. (Similar recrossing patterns are observed for 35 trajectories in the larger 263 water system in which 60% of the trajectories recrossed the barrier once, and no trajectories crossed more than twice.) This observation of significant recrossing implies a) that there is a serious deviation from simple Transition State Theory (TST),[5,6,29] which assumes all activated reactions proceed toward products with no recrossings of the barrier,[46] and b) that the accepted fundamental reaction "mechanism" along an average free energy reaction profile[5,6] needs to be reexamined.

The correction to the TST rate constant k^{TST} due to recrossings of the transition barrier is quantitatively given by the transmission coefficient

$$\kappa = \frac{k}{k^{TST}} , \tag{3.1}$$

where k is the true rate constant. We will compute only the correction to k^{TST} rather than the rate constant itself, as the latter requires a knowledge of the free energy of activation which is a computationally intensive calculation to perform using molecular dynamics.[32,47,48] In addition, it is κ that is a direct measure of the dynamical influence of the solvent in affecting the rate constant. Under the conditions in which trajectories are initialized on the transition barrier surface with initially forward momentum in the asymmetric stretch reaction coordinate, then run forward and backward in time from the initial conditions to determine the reaction beginning and outcome, the transmission coefficient κ is given by the Stable States Picture of reaction dynamics[15,49,50] as

$$\kappa = \frac{k}{k^{TST}} = \frac{\langle j_+ \, \theta[x(t)] \rangle_R - \langle j_+ \, \theta[x(-t)] \rangle_R}{\langle j_+ \rangle_R} , \tag{3.2}$$

where j_+ represents the initially positive flux across the transition barrier at time zero, $\theta[x(t)]$ is a step function for forward time dynamics which equals one on the product side and zero on the reactant side, $x(t)$ is the asymmetric stretch reaction coordinate defined to be zero at the transition barrier, $\theta[x(-t)]$ is a step function for reverse time dynamics which equals one on the product side and zero on the reactant side, and finally $\langle \, \rangle_R$ denotes an average over the equilibrium distribution, normalized by the reactant distribution. (See Ref. (15) for a more detailed discussion.) Each trajectory i in the equilibrium distribution has a particular probability w_i and some initial velocity v_i along the asymmetric reaction coordinate and is integrated out to 0.5 ps to determine the reaction fate. Thus, for N trajectories in the ensemble, κ translates to, and is computed as[15]

$$\kappa = \frac{\sum_{i,+}^{N} w_i \, |v_i| \, Q_i}{\sum_{i,+}^{N} w_i \, |v_i|} , \tag{3.3}$$

where + indicates all trajectories have initially positive velocity across the transition state surface and the value of Q_i depends on the initial and final states of the trajectory i,

$$Q_i = \begin{cases} +1 & \text{if Reactant} \rightarrow \text{Product} \\ 0 & \text{if Reactant} \rightarrow \text{Reactant or Product} \rightarrow \text{Product} \\ -1 & \text{if Product} \rightarrow \text{Reactant} . \end{cases} \tag{3.4}$$

For the 400 trajectories in the ensemble we compute κ to be 0.55. This represents a significant dynamical correction to the TST rate constant.

2. Recrossing Pattern Analysis

Figure 5 qualitatively illustrates the three predominant types of crossings observed: a) direct successful reactant → product (RP) transition with no recrossing (this is the only trajectory type in the TST description); b) a single recrossing reactant → product → reactant (RR) after the transition state is crossed in the forward direction and c) a single recrossing product → reactant → product (PP), in which the recrossing occurs prior to an initial reactant → product crossing. Why are there recrossings, and what is different for 1 crossing vs 2 crossing cases? We find that these features can be correlated with initial solvent configurations at the transition barrier and with the strength of the solvent-solute interaction.

A first indication of the strength of the reaction system-solvent coupling is revealed by examination of the time dependent friction,[11-13,50] $\zeta(t)$, which the solvent exerts on the reaction coordinate in the neighborhood of the transition barrier. This is computed by fixing the reaction system coordinates in a linear configuration at the gas-phase transition barrier and computing the time correlation of the fluctuating solvent forces resolved onto the normal-mode asymmetric-stretch reaction coordinate.[15,51] More explicitly, the time dependent friction is defined as

$$\zeta(t) = (\beta/\mu) \langle FF(t) \rangle , \tag{3.5}$$

in which F is the force acting on the asymmetric-stretch reaction coordinate with effective mass μ and $\beta^{-1} = k_B T$. Figure 6 shows that this force-force time correlation function has an initially fast decay out to 0.1 ps, followed by a short plateau region of duration approximately 0.025 ps, and then a slow decay toward zero. When the time dependent friction is computed on a typical bent geometry of 10° at the transition barrier, the result is the same as for the linear-geometry friction. We will return to this time dependence, as associated with solvent dynamics, but the major point here is that the initial magnitude of the friction

$$\zeta(t = 0) = (\beta/\mu) \langle F^2 \rangle \equiv \omega_\zeta^2 \tag{3.6}$$

indicates a very *strong* asymmetric stretch-solvent coupling, $\omega_\zeta \approx 890$ cm^{-1}, to be compared to the barrier frequency for the gas-phase potential ω_b of 460 cm^{-1}. Thus, it is not surprising that this strongly coupled solvent can induce recrossings even for a sharp intrinsic barrier.[11-13,50]

We now investigate the source of this strong coupling. A comparison calculation of ω_ζ for an isolated Cl^- ion in water gives $\omega_\zeta \approx 180$ cm^{-1}, so it seems reasonable to associate the strong solvent coupling noted above with a feature of the *reaction system*. The most likely association is with the charge migration in the reaction system along the reaction coordinate (Fig. 2). To verify this, a calculation of the time dependent friction on the reaction coordinate is made in which the charge migration along the reaction coordinate is made to pass through an inflection point (*cf* Fig. 7) at the transition barrier, thus giving a partial charge configuration, $Cl^{\delta-}$—$CH_3^{\delta+}$—$Cl^{\delta-}$ which is the same as before but which now has zero first derivative with respect to the reaction coordinate at the transition barrier. This calculation gives ω_ζ as 220 cm^{-1}, a significantly smaller value compared to the 890 cm^{-1} value above. It thus appears that the rate of change of charge along the reaction coordinate is indeed the key to the strong solvent forces experienced by the reaction system. We anticipated this result in Sec. II, where it was explained that an extra force between the reaction system and the solvent, in addition to the regular Coulombic force, arises from the migration of charge with motion along the reaction coordinate.

The critical character of the shifting charge distribution is further revealed by correlating the reaction fate with the Coulombic energy of interaction of the two chlorine atoms with the surrounding solvent at the transition barrier. For the 400 trajectories calculated, we find that the reaction outcome is largely determined by which of the two chlorine atoms is *best solvated* by the particular configuration of the surrounding solvent molecules at the transition barrier. For example, if the "left-hand" side chlorine has a more favorable interaction energy with the water as compared to the "right-hand" side chlorine, then the reaction tends to favor forming a "left-hand" side chloride ion, and this is true regardless of which way the momentum is initially headed along the reaction coordinate. The same is true for the opposite situation, in which the "right-hand" chlorine atom has some biased attractive potential energy with the solvent to form the ion, and does. In these two cases the trajectory recrosses the transition barrier once and forms the ion which is best solvated by the current solvent configuration. If products are favored then products are formed, and the product side is where the reaction begins (*cf* Fig 5c). If reactants are favored, then reactants are formed, and reactants are also where the reaction begins (*cf* Fig. 5b). Finally, we find that, if there is a sufficiently *symmetric* solvent potential with respect to either chlorine atom at the transition barrier, as if there were no particular preference by the solvent to have either the "left" or "right-hand" chloride ion formed then the reaction almost always proceeds from reactants to formation of products with *no* recrossing of the transition barrier (*cf* Fig. 5a).

Figure 8 illustrates these points in detail by showing, for ensembles of each of the three reaction outcomes described above and in Fig. 5, the average electric potential at the transition barrier at the "left-hand" chlorine atom, Cl, compared to the "right-hand" chlorine atom, Cl′, as a function of the radius of neighbor atoms included in the potential calculation. In addition, the average electric potential is computed for the sum of all three ensembles. This electric potential V is computed for a given radius r and a given chlorine atom i as

$$V_i(r) = \sum_{\{r_{ij} \le r\}} \frac{q_j}{r_{ij}} , \tag{3.7}$$

where r_{ij} is the distance between the chlorine atom i and solvent atom j and q_j is the charge on solvent atom j. Reactants are defined as $Cl + CH_3Cl'$, and products are defined as $ClCH_3 + Cl'$. Figure 8 shows that (a) there is a greater electric potential at "right-hand" chlorine atom, Cl′, for those reactions which cross the transition-state barrier twice from products to products (PP), and (b) a larger potential at Cl for reactions crossing the transition-state barrier twice from reactants to reactants (RR), but (c) no obvious difference in electric potential for the reactions which cross once from reactants to products (RP). Note that the average for all three reaction cases shows no average bias in favor of one of the chlorine atoms at the transition barrier, as is appropriate for an equilibrium ensemble.

Figure 8 also shows that the largest electrical potential difference for the PP and RR reactions occurs between 2.5 and 3.5 Å radially outward from the chlorine atoms and subsides to a nearly constant value thereafter. The onset at small neighbor distance of differences between the PP, RP, and RR cases shows that the local solvent configuration about the chloride ions largely determines the reaction outcome. A further indication of this is that the reaction dynamics are essentially the same for the small solvent system of 64 waters and the large 263 water system; the nearby electrical potentials are very similar for these two systems, and the fairly constant potentials at longer distance from the transition barrier apparently have little effect on the reaction fate.

All this suggests that the transmission coefficient can be approximately and usefully written as the contributions arising from one and two crossings,

$$\begin{aligned} \kappa &\approx \frac{1}{\langle j_+ \rangle_R} \left[\langle j_+ \theta[x(t)] \rangle_R^{(sym)} + \langle j_+ \theta[x(t)] \rangle_R^{(anysym)} - \langle j_+ \theta[x(-t)] \rangle_R^{(anysym)} \right] \\ &\approx \frac{\langle j_+ \theta[x(t)] \rangle_R^{(sym)}}{\langle j_+ \rangle_R} \\ &\approx \text{Prob}(sym) , \end{aligned} \tag{3.8}$$

where (*sym*) schematically indicates symmetric solvent configurations which always give rise to a

reactive trajectory, *i.e.* 1 crossing, while (*asym*) indicates asymmetric solvent configurations giving rise to 2 crossings and which never result in an overall reaction and thus yield zero net contribution to κ. This reduces κ to the first term which we have approximately expressed as Prob(*sym*), the relative probability for the "sufficiently" symmetric solvent configurations. Since that probability is less than unity, so is κ.

3. Frozen Solvent Nonadiabatic Solvation Model

Ultimately, it is the force exerted by the solvent on the reaction coordinate plus the internal force of the reaction system itself which drives the reaction toward its destiny. We have found above that the solvent potential energy bias between the two chlorine atoms at the transition barrier is a strong predictor of the outcome of the reaction. This strongly suggests that there is a force F_s due to biased solvent configurations, which may shift the location of the actual transition barrier and which acts along the reaction coordinate to drive the reaction one way or another. Little explicit information on a particular solvent configuration is obtained for this biased force from the calculation of the solvent friction using Eq. (3.5), since this gives an average square force for an ensemble of initial conditions. We can, however, examine the nature of the "true" total potential which defines the actual transition barrier for a particular solvent configuration as a perturbation from the gas-phase transition barrier. While a more detailed analysis is reserved for a companion paper,[22] a simple analysis suffices here to expose the key features. We begin by assuming a nonadiabatic frozen solvent model, *i.e.* that the solvent does not move appreciably on the time scale ~0.02 ps of the motion which decides the fate of the reaction process. Next the "true" potential $V_T(R)$ as a function of the reaction coordinate R which contains the potential due to the solvent plus that of the gas-phase reaction system, is expanded in a Taylor series about the gas-phase transition barrier location, $R = 0$,

$$V_T(R) = \sum_n \frac{R^n}{n!} \frac{\partial^n V_T}{\partial R^n} . \tag{3.9}$$

For simplicity, terms with order greater than two are discarded here. The zeroth order term $V_T(0)$ is the gas-phase potential energy at the transition barrier, modified by the interaction with the equilibrated solvent which lowers that energy (Fig. 4). Since $V_T(0)$ is already incorporated into the probability that we are at the transition barrier and that the molecular dynamics has selected the particular solvent configuration, we write the remaining effective potential referenced with respect to it as

$$V_{eff}(R) = R\frac{\partial V_T}{\partial R} + \frac{1}{2}R^2\frac{\partial^2 V_T}{\partial R^2} . \tag{3.10}$$

The first derivative of the gas-phase potential at $R = 0$ is zero at the saddle point. Thus only the frozen solvent force F_s contributes to the first derivative term,

$$F_s = -\frac{\partial V_T}{\partial R} , \tag{3.11}$$

while the second derivative contains contributions both from the gas-phase potential and from the frozen solvent,

$$\frac{1}{2}\frac{\partial^2 V_T}{\partial R^2} = -\frac{1}{2}\mu\omega_{b,na}^2 , \tag{3.12}$$

in which $\omega_{b,na}$ is a nonadiabatic frequency describing the force gradient acting on the reaction coordinate for a frozen solvent. The square nonadiabatic frequency is composed[22] of two contributions

$$\omega_{b,na}^2 = \omega_b^2 - (\Delta\omega)^2 , \tag{3.13}$$

involving the bare gas-phase barrier frequency ω_b and a solvent bias frequency $\Delta\omega$. The latter depends on the solvent configuration and will modify[22] the bare barrier. The solvent bias frequency reflects a solvent shift in the barrier curvature, as opposed to the solvent bias force F_s which shifts the barrier position (and, as we will see presently, its energy). As shown elsewhere,[22] the initial value of the time dependent friction is related to the average square solvent bias force

$$\zeta(0) = (\beta/\mu)\langle F_s^2 \rangle = \omega_\zeta^2 , \tag{3.14}$$

while $(\Delta\omega)^2$ depends on instantaneous solvent configurations.

The effective potential Eq. (3.10) at the gas-phase transition barrier can now be rewritten in the suggestive form

$$\begin{aligned} V_{eff}(R) &= -\frac{1}{2}\mu\omega_{b,na}^2 R^2 - F_s R \\ &= -\frac{1}{2}\mu\omega_{b,na}^2\left[R + \frac{F_s}{\mu\omega_{b,na}^2}\right]^2 + \frac{F_s^2}{2\mu\omega_{b,na}^2} . \end{aligned} \tag{3.15}$$

This shows that the location R of the instantaneous solvent dependent transition barrier is shifted away from the equilibrium transition barrier (which corresponds in location to that of the gas-phase transition barrier $R = 0$) by an amount

$$\Delta R = -\frac{F_s}{\mu\omega_{b,na}^2} , \tag{3.16}$$

while the shift in energy from the equilibrium transition barrier value $V_T(0)$ is

$$\Delta V = \frac{F_s^2}{2\mu\omega_{b,na}^2} . \tag{3.17}$$

These features are illustrated in Fig. 9, in which the solvent bias potential shifts the barrier by ΔR in position along the reaction coordinate and, very importantly, by ΔV in energy relative to the equilibrium transition barrier. The shift in energy is always greater than or equal to zero with respect to the equilibrium transition barrier, while the transition barrier will shift left or right depending on the nature of the particular solvent configuration. We will presently employ this simple description to characterize both the crossing patterns and κ in detail.

There is a central assumption in our frozen solvent description above that the solvent configuration does *not* undergo any appreciable change in the time required for the reaction fate to be decided. This is in fact reasonable, considering that the characteristic time scale[50] on a barrier of frequency $\omega_b = 461$ cm^{-1} is $2\omega_b^{-1} = 0.02$ ps. ($2\omega_b^{-1}$ is the time required for a thermal trajectory to decrease its potential energy $2k_BT$ below the barrier top.) On this short time scale, the solvent does not move into a significantly different configuration, and any bias (or lack of bias) in potential with respect to the two chlorine atoms does not break down appreciably before the reaction fate is decided. This is also in accord with the minor variation of $\zeta(t)$ on a time scale of approximately 10^{-2} ps (*cf* Fig. 6). As this bias is primarily associated with the charge-dipole electric potential (*cf* Fig. 8), the only thing which could break the bias would be a reorientation or a significant change in the water dipoles within the time required for barrier crossing. The only solvent motions which can occur on this brief time scale are the internal vibrations described by the symmetric and asymmetric stretches and bending motions of water, with normal mode frequencies of 3832 cm^{-1}, 3943 cm^{-1} and 1649 cm^{-1} respectively.[52] However, these vibrations do not affect the orientations of the water dipoles as much as water molecule rotational motions do, and the gross rotational motions are slow on the time scale for barrier crossing.

Both of these aspects are illustrated in the time dependent friction Fig. 6 and in Fig. 10, which shows a calculation of the rotational time correlation functions for pure flexible water solvent at 298 K. A comparison of Fig. 10 with the time dependent friction correlation function in Fig. 6 shows a remarkable similarity between the two characteristic decay times and profiles. Both correlation functions have an initial fast decay, followed by a small rise, and then a long, slow decay. It would appear likely that the major time development of the time dependent friction is strongly related to the rotational motions of the water solvent, and this seems reasonable in light of the observation that the strong coupling between the solvent and reactions system is largely due to the charge-dipole forces, which change most significantly with water rotational motions. Thus, the rotational motions of the waters do not effect a major change in the solvent configuration on the time scale for barrier crossing; rather, the solvent is seen to move on a much longer time scale *after* the decision has been made concerning the reaction outcome by the instantaneous configurations of the water molecules.

4. Analysis of κ

The features of the solvent bias described above are revealed in the dynamics because those trajectories which have an asymmetric solvent configuration and recross the gas-phase transition state barrier are seeing an effective potential in which the reaction system is not really at the "true" instantaneous solvent configuration dependent transition barrier defined by the effective potential [Eq. (3.15)]: rather they are shifted from that location by an amount ΔR in position [Eq. (3.16)] and different in energy by an amount ΔV [Eq. (3.17)]. Thus, the particular trajectory must either have extra kinetic energy along the reaction coordinate equal to ΔV in order to react, or face an effective barrier which sends it back (*i.e.*, recrosses) down the potential. On the other hand, those trajectories which have a solvent configuration which produces a solvent potential which does not lead to an appreciable ΔV will usually have enough kinetic energy to react without recrossing. This suggests the following analysis.

Since the effective potential is shifted higher in energy by an amount ΔV depending on solvent configuration, a trajectory would require at least that much kinetic energy in the asymmetric stretch to overcome the barrier and make a successful crossing. This suggests that a plot of the reaction outcome for a given kinetic energy in the reaction coordinate vs ΔV should show that those trajectories which have kinetic energy in excess of ΔV will be successful, while those with less kinetic energy will not. This idea is investigated in a calculation in which a subset of 100 initial reaction system configurations are randomly selected from the ensemble of 400 initial conditions and, for each initial condition, random positive values of the asymmetric stretch momentum are chosen from a uniform energy distribution. The trajectories are then run long enough to determine whether or not they will recross the barrier. These 1000 trajectories are represented as points on a "correlation" plot in Fig. 11, which shows the reaction outcome for the various values of kinetic energy in the reaction coordinate vs the additional frozen solvent corrected barrer ΔV. Here, individual trajectories are labeled with '+', 'O', or 'Δ', depending on whetrherthey cross the transition barrier once from reactants to products (RP), cross twice from reactants to reactants (RR, $\Delta R > 0$), or cross twice from products to products (PP, $\Delta R < 0$), respectively. These different cases, according to the frozen solvent model, should be, and mostly are partitioned into regions which are separated by a line of slope 1, dividing the RP and RR trajectories, and a line of slope -1, dividing the RP and PP trajectories. The lines of slope 1 and -1 indicate the threshold kinetic energy in the asymmetric stretch required by a trajectory to cross the additional barrier of height ΔV. This figure shows that the outcome of the reaction is indeed largely determined by the conditions of the reaction system and the instantaneous configuration of the solvent at the gas-phase transition barrier. Thus, we only need a knowledge of the initial kinetic energy in the asymmetric stretch reaction coordinate and the shifted barrier height ΔV (determined by the gas-phase potential added to the frozen solvent potential due to the solvent configuration at the gas-phase transition barrier) to predict what the likely outcome of the reaction will be *without the need to run dynamics away from the gas-phase transition barrier.*

The transmission coefficient κ can also be predicted without running any dynamics, except on the transition barrier, from a knowledge of the ensemble of solvent configurations of the system with the reacting atoms located on the transition barrier. This was first indicated by Eq. (3.8), in which κ is related to the relative probability for finding a symmetric solvent configuration about the two chlorine atoms at the transition barrier. Now we include the effect of having kinetic energy in the asymmetric stretch reaction coordinate, which may overcome the additional barrier height ΔV and result in a successful reaction. The relevant probability for a successful reaction given ΔV is[22]

$$\mathrm{P(reaction}\,|\,\Delta V) = e^{-\beta\Delta V}\,, \tag{3.18}$$

and κ, the probability for a successful reaction in the ensemble of initial conditions on top of the equilibrium barrier, is the average

$$\kappa = \mathrm{P(reaction)} = \langle\, e^{-\beta\Delta V}\, \mathrm{P}(\Delta V)\,\rangle\,, \tag{3.19}$$

in which $\mathrm{P}(\Delta V)$ is the probability for having a particular biased solvent configuration which gives rise to an energy shift ΔV. This average can be performed using the MD ensemble of initial conditions, and using Eqs. (3.11), (3.12) and (3.17) to determine ΔV. The result is $\kappa = 0.47 \pm 0.05$ which is in satisfactory agreement with the value $\kappa = 0.55 \pm 0.05$ determined by direct MD simulation.

In fact, an analytic theory for κ in the frozen, nonadiabatic solvent limit presented in the companion paper[22] based on the general van der Zwan-Hynes nonequilibrium solvation rate theory[12,13] predicts that

$$\kappa = \sqrt{\frac{1}{1 + 2\beta \langle \Delta V \rangle}} , \tag{3.20}$$

where the average barrier shift is $\langle \Delta V \rangle$. The average $\beta \langle \Delta V \rangle$ is determined from MD simulation at the transition barrier to be 1.92, yielding $\kappa = 0.45$, again in good agreement.

In summary, the frozen solvent, nonadiabatic perspective appears to give both a qualitatively and quantitatively accurate picture of the model S_N2 reaction mechanism and rate.

Finally, we have stressed throughout this paper the critical importance of the short time scale dynamics for the reaction; Eq. (3.20) for κ is an explicit example of this, since it involves only a static average for a frozen solvent. It is of interest to ask what the prediction of Kramers theory[53] for κ would be. In this theory, the fully time integrated friction of Fig. 6 enters as the friction constant

$$\zeta = \int_0^\infty dt\, \beta/\mu \langle FF(t) \rangle = \omega_\zeta^2 \tau , \tag{3.21}$$

in the Kramers transmission coefficient,

$$\begin{aligned} \kappa &= \sqrt{1 + (\zeta/2\omega_{b,eq})^2} - (\zeta/2\omega_{b,eq}) \\ &\approx \omega_{b,eq}/\zeta , \end{aligned} \tag{3.22}$$

for high friction. Here $\omega_{b,eq}$ is the mean barrier frequency[22] which we estimate as roughly 990 cm^{-1}. (This value is from our companion paper.[22]) The friction constant is approximately $\zeta = \omega_\zeta^2 \tau$, while ω_ζ is the square root of the initial friction value of 890 cm^{-1} from Eq. (3.6), and τ is the lifetime of the force correlations, estimated from Fig. 6 as $\tau \approx 1$ ps. This gives the Kramers prediction of $\kappa = 0.007$, catastrophically far below the actual $\kappa = 0.55$. The long time scale integrated friction in the Kramers picture is able to induce significant amounts of barrier recrossing, resulting in a diffusion controlled barrier passage and a minuscule κ value. Clearly, the long time scale friction is completely irrelevant on the short time scale during which the reaction fate is decided.[11-13,51,54]

5. Energy relaxation

We now return to the question of why there are *only* 1 or 2 crossings of the transition barrier (*i.e.* virtually no observed instances of more than 2 sequential barrier crossings). Here we examine the time scales for which the incipient products are energetically stabilized in the solvent. Figure 12 shows the internal energy of the reaction system as a function of time, in which the energy is partitioned into $[Cl—CH_3—Cl]^-$ potential energy plus $CH_3—Cl$ vibrational kinetic energy, $CH_3—Cl$ rotational kinetic energy, and the translational kinetic energies of the $CH_3—Cl$ molecule and of the Cl^- ion.

The key feature here is that, in approximately 0.025 ps before and after the transition barrier, the total energy in the reaction system increases by approximately one kcal/mol, and then is *rapidly* dissipated into the solvent at somewhat longer times. This initial increase in energy and subsequent loss is primarily associated with the $CH_3—Cl$ vibrational kinetic energy (*cf* Fig. 12). Note that although the figure shows the $[Cl—CH_3—Cl]^-$ potential energy plus $CH_3—Cl$ vibrational kinetic energy, the increase in energy shortly before and after the transition barrier is associated with vibrational kinetic energy, and not due to any increase in the total potential energy. It is another example of the effects of the shifting charge on the dynamics as the incipient Cl^- ion accelerates off the transition barrier into a more favorable ionic interaction with the surrounding waters, initially causing the $CH_3—Cl$ to "form" more rapidly compared to the gas phase and thus increasing its vibrational kinetic energy. The subsequent loss of excess vibrational energy to the solvent at longer times (≥ 0.1 ps) occurs very rapidly (We have verified that this is largely independent of the presence of the charge switching.). This is in marked contrast to the energy decay patterns observed in the gas phase in Fig. 3, and is also quite different from that found for the A + BC reaction in rare gas solvents.[15] Thus, the picture is that the initial solvent configuration can result in no, or a very small number of recrossings, and once the

incipient species favored by the extant conditions is formed, very rapid stabilization ensues.

The observations above raise interesting questions for future study about the vibrational relaxation of polar molecules in polar solvents. But first and foremost they demonstrate that the reaction dynamics are quintessentially a question of both "intrinsic" reaction system and solvent dynamics. The stabilization observed intimately involves the solvent, yet the time scale is so short that dynamics, and not equilibrium solvation, is critical. Our results show that the relaxation is not occurring on the monotonically decreasing mean potential (*cf* Fig. 4). Rather, rapid stabilization occurs in the complex well on a subpicosecond time scale due to the strong interaction with the solvent. It is only subsequent to this that solvent dipole reorientation on a picosecond time scale (*cf* Fig. 10) will occur to "solvate" the complex and establish the mean potential features of Fig. 4 in the neighborhood of the products.

IV. Variation of Solvent, Barrier Height and Charge Switching

In this section we explore the effect of variation of solvent, barrier height and charge switching to examine the reaction dynamics under different conditions and to determine a range of reaction conditions over which the nonadiabatic frozen solvent model applies, and some conditions for which this model breaks down. Table 4 presents the results of this section (see below) and of Sec. III above.

A. Variation of Mass of Solvent Hydrogens

The picture of this S_N2 reaction which emerges is that the reaction dynamics, insofar as the reaction outcome is concerned, are largely *independent* of the solvent dynamics for all but the least sharp (5 kcal/mol) barrier (see below). We can test this if we slow down the solvent vibrational motions and rotational reorientation time by replacing the mass of the hydrogens on water by the mass of oxygen, but leaving all other variables in the system unchanged. In this way we change the short time aspects of the time dependent friction, *i.e.* slow down the initial decay in the correlation function (*cf* Fig. 13), but the initial value of the friction is unchanged, since that is a static quality independent of the solvent mass. Thus, we make the waters even more "frozen" by slowing down their rotational, vibrational, and translational motions. We find that the reaction dynamics (*e.g.*, recrossing patterns), and the energy decay patterns remain essentially the same as with the H_2O case, and κ (*cf* Table 4) matches the frozen solvent, nonadiabatic model prediction. The fact that our reaction dynamics in the H_2O solvent system behaves so similarly to the reaction dynamics in an even more frozen solvent system further buttresses the frozen solvent picture we have developed.

B. Variation of Barrier Height

The frozen nonadiabatic solvent picture of the reaction suggests two predictions for the consequences of varying the central S_N2 barrier height.

First, for higher and sharper barriers, since the bare barrier frequency ω_b is increased, the reaction time scale $\sim 2\omega_b^{-1}$ is diminished, and the frozen solvent scenario should be even more accurate. Further, the stronger intrinsic driving force for the reaction should more easily dominate solvent opposition and κ should rise. This is apparent from Eqs. (3.13), (3.17) and (3.20). Increasing ω_b increases the nonadiabatic frequency, $\omega_{b,na}^2$, which in turn decreases the average energy shift $\langle \Delta V \rangle$ (*cf* Fig. 9). Thus, κ will increase according to Eq. (3.20). This prediction is confirmed in Table 4 for a 31.9 kcal/mol central barrier.

Second, if the barrier height is lowered, concomitantly lowering the bare barrier frequency, we expect κ to diminish in the nonadiabatic solvent picture. But unfortunately the entire basis for the frozen solvent description is mooted by the longer time scale for the reaction and the associated motion of the solvent molecules. We thus expect a serious breakdown in the frozen solvent description, and Table 4 amply demonstrates this point for a 5 kcal/mol barrier. For this case we find that $\omega_{b,na}^2$ (*cf* Eq. 3.13) is in fact *negative* for a significant fraction of solvent configurations. This means that there is a "polarization cage" along the reaction coordinate as described by van der Zwan and Hynes,[11-13] and a different analysis is required.

We intend to return to the low barrier case in a subsequent study and analyze the role of the solvent motions in detail for the case in which they are on the same time scale as the effective motion

along the reaction coordinate.

C. Variation of the Rate of Charge Switching

As seen in Sec. III, the variation of charge along the reaction coordinate has a dominant effect on the solvent friction and on the reaction dynamics. In a further series of calculations, we have determined that slowing this charge variation down reduces the number of trajectories which recross, the amplitude of the time dependent friction, and the energy pickup in vibration shortly after the transition state.

Here we discuss explicitly only the transmission coefficient κ as a function of the rate of charge variation. In the nonadiabatic solvent perspective, κ is determined from Eq. (3.20) by the average solvent induced barrier shift $\langle \Delta V \rangle$ which by Eq. (3.17) is quadratically sensitive to the solvent bias force F_s. For reduced rates of charge variation, this force will diminish. Thus, $\langle \Delta V \rangle$ will decrease and κ will rise. Similarly, for an increased rate of charge switching, κ is expected to decrease.

These predictions are verified in Table 4. The rate of charge switching can be varied by adjusting the parameter κ_1 in the charge switching function (*cf* Appendix A). Changing this parameter by a scale factor x changes the rate of charge switching by the same factor. When the rate of switching of the charge along the reaction coordinate is decreased by a factor of two, κ is 0.73. This is slightly larger than the result $\kappa = 0.55$ for the full switching. Clearly, the effect is fairly robust. If we decrease the charge switching rate by a factor of eight, then κ rises to 0.87; significantly less recrossing occurs. A correlation plot is presented for this case in Fig. 14. This diagram shows that the range of ΔV for this reduced rate of charge switching is much less than that for the normal rate of charge switching correlation (*cf* Fig. 11), as predicted by the above argument. The reaction is approaching the "weak solvation limit"[12,13] in which the solute-solvent interaction is sufficiently weak so that passage over a sharp barrier is negligibly perturbed. (Calculations for the case of no charge switching close to the transition state give similar results as for the 1/8'th charge switching, $\kappa = 0.90$. This calculation requires a different functional form to describe the charge switching (*cf* Fig. 7).) Again the analytic prediction gives an excellent description, documented in Table 4.

D. Collapsed Charge Model

All of our reaction dynamics have been computed for the united atom definition in which the charges on the hydrogen atoms and the carbon atom of the methyl group are reduced to a single positive charge on the central atom. In forming the united atom, the effect of the hydrogen atoms extending into the surrounding solvent with their associated charges is lost, and this may result in the hydrogens of the water solvent moving in unusually close to the chlorine atoms at the transition state in a effort to maximize the attractive coulombic energy. Up to now, all dynamics have been computed for a charge distribution which has a slightly lower positive charge on the central united atom than would be given by the united atom approximation to Jorgensen's potentials[8,9] (*cf* Appendix A and Fig. 2). As explained in Appendix A, we feel that this is a reasonable distribution to mimic the reaction system-solvent interaction when the CH_3 group in the S_N2 system is collapsed to a united atom. (This view is supported by the agreement for the model noted in Sec. II.3 with the radial distribution functions computed by Jorgensen.[8,9]) Still, the dynamics without this slight positive charge diminution are of interest. We have determined that the dynamics for the united atom system without this slight charge redirection (*cf* Fig. 15) are similar to those with it, but κ is only 0.30. In addition, there are "polarization cage" effects[11-13] as seen for the low 5 kcal/mol barrier dynamics (see above), and the frozen solvent picture no longer applies. This further reduction in κ is expected, given the increased chlorine-solvent interaction likely in this calculation (*cf* Appendix A).

V. Conclusions

Molecular dynamics have been computed for a model S_N2 reaction in solution, and the fundamental reaction picture is found to be significantly different from that painted by a standard free energy equilibrium solvation picture of solvent effects. The free energy description treats the solvent as a system which is always equilibrated to the reaction system at all points along the reaction coordinate, and the solvent accordingly affects only the free energy profile of the reaction coordinate through

Table 4. Transmission Coefficients from Molecular Dynamics and Frozen Solvent										
Barrier Height (kcal/mol)	Barrier frequency (cm^{-1})	Relative Rate of Charge Switching	Solvent type	# of mol.	Molecular Dynamics κ_{MD}	# of traj.	error	Frozen Solvent Model κ_{FSM}*	# of traj.	error
13.9	461.2	1.0	H_2O	64	0.55	400	±0.05	0.45	400	±0.05
13.9	461.2	1.0	H_2O	263	0.64	50	±0.13	0.51	50	±0.13
13.9	461.2	1.0	O_2O	64	0.44	100	±0.10	0.46	100	±0.08
31.9	893.6	1.0	H_2O	64	0.74	100	±0.09	0.74	100	±0.09
4.9	231.7	1.0	H_2O	64	0.40	100	±0.10	0**	100	---
13.9	461.2	2.0	H_2O	64	0.38	400	±0.05	0.26	400	±0.04
13.9	461.2	0.5	H_2O	64	0.73	400	±0.04	0.67	400	±0.06
13.9	461.2	0.125	H_2O	64	0.90	400	±0.03	0.87	400	±0.03
13.9	461.2	0.0	H_2O	64	0.91	400	±0.03	0.91	400	±0.02
13.9	461.2	1.0***	H_2O	64	0.31	100	±0.10	0**	100	---

* $\kappa_{FSM} = (1+\beta\langle\Delta V\rangle)^{-1/2}$, Eq. (3.20).
** A serious breakdown of the theory, see text.
*** Collapsed charge model, see text.
The estimated errors for the κ_{MD}'s are calculated using a multinomial cell probability analysis and a 95% confidence interval, the κ_{FSM}'s, from a propagation-of-errors method.[55]

equilibrium solvation and stabilization of the intermediates. It also implies that simple TST is a good description for the reaction since only the free energy profile of the reaction coordinate is changed by the solvent.

We find serious deviations from this picture in our model study. Transition State Theory breaks down markedly, as recrossings of the transition state surface are observed. The reaction outcome is highly dependent on the local configuration of the solvent at the transition state; in fact, it is in significant measure *determined* by that configuration. The reaction in the transition barrier neighborhood is characterized by nonadiabatic solvation,[11-13] *i.e.* frozen solvent configurations, rather than the adiabatic equilibrium solvation envisaged in simple TST.

This central feature has two sources. The first is that the time scale during which the reaction fate is determined is significantly shorter than the characteristic time scale of solvent reorientation. Thus, reactions occur in a "frozen solvent" at the transition barrier. The second is that there is a rapid variation of charge distribution along the reaction coordinate close to the transition barrier, and this leads to pronounced coupling between the S_N2 system and the water solvent.

The location of the transition barrier for a particular solvent configuration can shift markedly from the gas phase barrier in height and position along the reaction coordinate. This shift is not accounted for in the equilibrium solvation free energy picture which assumes that the transition state has the same location as in the gas phase reaction, but is shifted uniformly down in energy.

Instead we find that there are solvent configuration dependent transition barriers shifted up in energy from the equilibrium value. These shifts have been correlated with asymmetric "solvation" in which one of the chlorines in the S_N2 transition state is differentially stabilized by the solvent, and the connection to the observed recrossing patterns has been made in considerable detail.

A simple frozen solvent, nonadiabatic solvation theory for predicting the outcome of, and the transmission coefficient for a solution reaction based on the solvent configuration at the equilibrium transition state is given, in which there is no need to compute any dynamics except at the transition barrier. This theory is tested over a wide range of reaction system variables and found to be in good agreement with our MD simulation results. In contrast, a Kramers description fails dramatically. We find, however, that this simple theory breaks down (as expected) in certain regimes, for example, with low barrier heights and barrier frequencies. The full analysis of these regimes is a subject for future investigation.

We find in our model system that vibrational energy transfer of the nascent products to the polar solvent is quite rapid. This is another example that on the molecular level the mechanism of the reaction process is not determined by motion on the mean potential free energy surface, but rather requires an investigation of the dynamics to reveal its essential features.

Finally, our predictions of a transmission coefficient correction $\kappa = 0.55$ for the 13.9 kcal/mol model $Cl^- + CH_3Cl$ reaction in H_2O could fairly be interpreted as having only a modest quantitative effect on the overall reaction rate constant,[56,57] whose solvent influence is dominated by the large solvation free energies of the reactants, products and transition state.[1-10] This perfectly valid perspective, however, does not take into account that, according to our study, the molecular-level "mechanism" of the reaction, and the solvent participation therein differs fundamentally from the standard conception. Further, it is likely that significantly smaller κ values – and hence larger numerical deviations from the equilibrium solvation TST rate constant – will occur for lower barrier S_N2 reactions (*cf* Sec. IV.B). We hope to report in the future on studies of this regime, as well as on related matters such as alternate descriptions[58,59] of the charge variation along the reaction coordinate.

ACKNOWLEDGMENTS

Acknowledgment is made to the donors of the Petroleum Research Fund, administered by the American Chemical Society, for partial support of this research. This work was also supported by grants CHE 84-19830 (JTH) and CHE 84-07491-02 (KRW) from the National Science Foundation (Chemistry), and by the Office of Naval Research (Chemistry).

APPENDIX A

The non-bonded interactions between the water solvent and the solute, $[Cl{-}{-}CH_3{-}{-}Cl]^-$, are described by a Lennard-Jones Coulomb (LJC) potential in which the charge on the solvent atoms is fixed while the charge on the solute atoms varies as a function of reaction progress to model the charge switching process. This total non-bonded potential is

$$V^{NB} = \sum_{j=1}^{n} V_j^{NB} , \tag{A1}$$

where

$$V_j^{NB} = \sum_{i=A}^{C} \left\{ \frac{Q_{ij}^2}{r_{ij}} + \frac{A_{ij}}{r_{ij}^{12}} - \frac{B_{ij}}{r_{ij}^{6}} \right\} + V_j^{Water}(r_{j,1}, \ldots, r_{j,j-1}, r_{j,j+1}, \ldots, r_{j,n}) , \tag{A2}$$

in which $r_{ij} = r_i - r_j$ is the distance between solute atom i and solvent atom j, n is the number of solvent atoms, the three solute atoms are denoted by Cl = A, CH_3 = B, Cl′ = C, Q_{ij} is the charge, A_{ij} and B_{ij} are the Lennard-Jones constants, and V^{Water} is the water solvent intermolecular potential.[21]

The charge and Lennard-Jones parameters, Q_{ij}, A_{ij}, B_{ij}, are composed of multiplicative factors of the specific solvent and solute parameters as follows. Let

$$Q_{ij}^2 = q_i q_j , \tag{A3}$$

$$A_{ij} = a_i a_j \,, \tag{A4}$$

and

$$B_{ij} = b_i b_j \,, \tag{A5}$$

where q_i, a_i, b_i are solute parameters and q_j, a_j, b_j are solvent parameters, then Eq. (A2) becomes

$$V_j^{NB} = \sum_{i=A}^{C} \left\{ \frac{q_i q_j}{r_{ij}} + \frac{a_i a_j}{r_{ij}^{12}} - \frac{b_i b_j}{r_{ij}^{6}} \right\} + V_j^{W \neq \alpha}(r_{j,1}, \ldots r_{j,j-1}, r_{j,j+1}, \ldots r_{j,n}) \,. \tag{A6}$$

The charge switching is modeled by allowing the charge, q_i, on the solute atoms to vary as a function of reaction progress in a fashion similar to the one-dimensional charge switching prescription of Jorgensen,[8] although our reaction progress is conveniently defined to be $(r_{AB}^2 - r_{BC}^2)$ to allow for a full three-dimensional description of the charge switching. In addition the Lennard-Jones parameters a_i and b_i can also be made variable with reaction progress such that

$$q_i \equiv q_i(r_{AB}^2 - r_{BC}^2) \,, \tag{A7}$$

$$a_i \equiv a_i(r_{AB}^2 - r_{BC}^2) \,, \tag{A8}$$

and

$$b_i \equiv b_i(r_{AB}^2 - r_{BC}^2) \,. \tag{A9}$$

The force on the k^{th} solute atom due to solvent interaction is given by

$$\begin{aligned} \mathbf{F}_k^{NB} &= \frac{-\partial V^{NB}}{\partial \mathbf{r}_k} \\ &= \sum_{j=1}^{n} \left\{ \frac{q_k q_j}{r_{kj}} + 12\frac{a_k a_j}{r_{kj}^{12}} - 6\frac{b_k b_j}{r_{kj}^{6}} \right\} \frac{\mathbf{r}_{kj}}{r_{kj}^2} \\ &\quad - \sum_{j=1}^{n} \sum_{i=A}^{C} \left\{ \frac{q_j}{r_{ij}} \frac{\partial q_i}{\partial \mathbf{r}_k} + \frac{a_j}{r_{ij}^{12}} \frac{\partial a_i}{\partial \mathbf{r}_k} - \frac{b_j}{r_{ij}^{6}} \frac{\partial b_i}{\partial \mathbf{r}_k} \right\} \\ &= \sum_{j=1}^{n} \left\{ \frac{q_k q_j}{r_{kj}} + 12\frac{a_k a_j}{r_{kj}^{12}} - 6\frac{b_k b_j}{r_{kj}^{6}} \right\} \frac{\mathbf{r}_{kj}}{r_{kj}^2} \\ &\quad - \sum_{j=1}^{n} \sum_{i=A}^{C} \left\{ \frac{q_i' q_j}{r_{ij}} + \frac{a_i' a_j}{r_{ij}^{12}} - \frac{b_i' b_j}{r_{ij}^{6}} \right\} \nabla_k(r_{AB}^2 - r_{BC}^2) \,. \end{aligned} \tag{A10}$$

Notice that the solute charge and Lennard-Jones parameters are differentiated with respect to $\mathbf{r}_k$ since these are now variable with the reaction progress. These terms are expanded as follows.
For $g = q,a,b$; i,k = A,B,C

$$\frac{\partial g_i}{\partial \mathbf{r}_k} = \frac{\partial g_i}{\partial(r_{AB}^2 - r_{BC}^2)} \nabla_k(r_{AB}^2 - r_{BC}^2) = g_i' \nabla_k(r_{AB}^2 - r_{BC}^2) \,, \tag{A11}$$

in which the explicit gradients of $(r_{AB}^2 - r_{BC}^2)$ are

$$\nabla_A(r_{AB}^2 - r_{BC}^2) = 2\mathbf{r}_{AB} \,, \tag{A12}$$

$$\nabla_B(r_{AB}^2 - r_{BC}^2) = 2\mathbf{r}_{CA} \,, \tag{A13}$$

and

$$\nabla_C(r_{AB}^2 - r_{BC}^2) = 2\mathbf{r}_{BC} \,. \tag{A14}$$

Definition of the new variables

$$A_j = 2 \sum_{i=A}^{C} \left\{ \frac{q_i' q_j}{r_{ij}} + \frac{a_i' a_j}{r_{ij}^{12}} - \frac{b_i' b_j}{r_{ij}^{6}} \right\} \tag{A15}$$

and

$$\Gamma_{ij} = \left\{ \frac{q_i q_j}{r_{ij}^3} + 12\frac{a_i a_j}{r_{ij}^{14}} - 6\frac{b_i b_j}{r_{ij}^8} \right\} \tag{A16}$$

allows us to write the non-bond forces on the solute atoms due to the jth solvent atom in terms of Λ_j and Γ_{ij} as

$$\mathbf{F}_{Aj}^{NB} = \Gamma_{Aj}\mathbf{r}_{Aj} - \Lambda_j\mathbf{r}_{AB} , \tag{A17}$$

$$\mathbf{F}_{Bj}^{NB} = \Gamma_{Bj}\mathbf{r}_{Bj} - \Lambda_j\mathbf{r}_{CA} , \tag{A18}$$

and

$$\mathbf{F}_{Cj}^{NB} = \Gamma_{Cj}\mathbf{r}_{Cj} - \Lambda_j\mathbf{r}_{BC} . \tag{A19}$$

Here, Λ_j is of the same form as the first term of V_j^{NB}, except that q_i, a_i, and b_i are replaced by $2q_i'$, $2a_i'$, and $2b_i'$, respectively. Also note that $\Gamma_{ij}\mathbf{r}_{ij}$ is just the normal LJC force. Summing over all the solvent atom interactions, the total force on each solute atom is then

$$\mathbf{F}_A^{NB} = \sum_{j=1}^{n} \mathbf{F}_{Aj}^{NB} = \sum_{j=1}^{n} \left\{ \Gamma_{Aj}\mathbf{r}_{Aj} - \Lambda_j\mathbf{r}_{AB} \right\}, \tag{A20}$$

$$\mathbf{F}_B^{NB} = \sum_{j=1}^{n} \mathbf{F}_{Bj}^{NB} = \sum_{j=1}^{n} \left\{ \Gamma_{Bj}\mathbf{r}_{Bj} - \Lambda_j\mathbf{r}_{CA} \right\}, \tag{A21}$$

and

$$\mathbf{F}_C^{NB} = \sum_{j=1}^{n} \mathbf{F}_{Cj}^{NB} = \sum_{j=1}^{n} \left\{ \Gamma_{Cj}\mathbf{r}_{Cj} - \Lambda_j\mathbf{r}_{BC} \right\}. \tag{A22}$$

Our adopted functional form for the solute LJC parameters, (q_i, a_i, b_i), is, for $g \equiv q,a,b$ and i = A,B,C,

$$\begin{aligned} g_i &\equiv g_i(r_{AB}^2 - r_{BC}^2) \\ &= \alpha_{ij}^g f_1(r_{AB}^2 - r_{BC}^2) + \beta_{ij}^g f_2(r_{AB}^2 - r_{BC}^2) + \gamma_i^g \\ &= \alpha_{ij}^g f_1 + \beta_{ij}^g f_2 + \gamma_i^g , \end{aligned} \tag{A23}$$

in which f_1 is an odd function

$$f_1(r_{AB}^2 - r_{BC}^2) = \tan^{-1}\kappa_1(r_{AB}^2 - r_{BC}^2) , \tag{A24}$$

and f_2 is an even function

$$f_2(r_{AB}^2 - r_{BC}^2) = \frac{1}{\kappa_2(r_{AB}^2 - r_{BC}^2)^2 + 1} . \tag{A26}$$

Similarly, the derivatives for $g = q,a,b$; i = A,B,C are

$$g_i' = \alpha_{ij}^g f_1' + \beta_{ij}^g f_2' , \tag{A27}$$

$$f_1' = \frac{\kappa_1}{\kappa_1^2(r_{AB}^2 - r_{BC}^2)^2 + 1} , \tag{A28}$$

and

$$f_2' = \frac{-2\kappa_2(r_{AB}^2 - r_{BC}^2)}{(\kappa_2(r_{AB}^2 - r_{BC}^2)^2 + 1)^2} . \tag{A29}$$

We choose these functions rather than Jorgensen's functions[8,9] because of the non-differentiability of the latter at the transition state as well as the requirement for defining these functions for the three-dimensional space in which we calculate dynamics. We have found it feasible to use a piecewise fifth degree polynomial fit to these functions and their derivatives when we actually perform the dynamical calculations.

The central atom is modeled as a united CH_3 group, which is given the diameter of a methyl group (4.25 Å) and contains no explicit hydrogens. There is some question of how the charges on the individual hydrogen and carbon atoms should be summed and collapsed down to form a single partial positive charge on the central united atom. In forming the united atom, the effect of having the hydrogen atoms sticking out in the solvent with their partial positive charges is lost, and this may allow the hydrogen atoms of the water molecules to move unusually close to the two chlorine atoms at the transition state to maximize the attractive potential energy. To compensate for the loss of the repulsion force between hydrogens of the methyl group which would keep the hydrogens of the waters from coming too close to the chlorine atoms, an effective reduction in the negative charge of the chlorine atoms at the transition state is required to lower the attractive potential. Reducing the amount of negative charge on the chlorine atoms at the transition state means that the central atom must carry more of the partial negative charge so that total charge conservation is maintained. This results in the central atom having a slightly less positive charge than is predicted by the united atom definition of summing the charges of the methyl and collapsing them down to a single charge. The charge switching parameters are determined first for the united atom approximation, which gives an overall reasonable fit to Jorgensen's one-dimensional functions,[8] with $\kappa_1 = 0.75$ and $\kappa_2 = 0.25$. Then the β_i^q parameters are adjusted so that the charge on the central group decreases (becomes less positive) at the transition state, and the α_i^q parameters are chosen to match the dipole moment of the separated CH_3Cl molecule as described by Jorgensen.[8] Figure 2 illustrates the variation of charge on the three atoms of the reaction system as a function of the reaction progress, $(r_{AB}^2 - r_{BC}^2)$, and Table A1 gives the parameters. The charge variation for the Jogensen methyl charges collapsed down onto a single, united atom are shown in Fig. 15.

The nonvariable charges on the water atoms are chosen from Watts,[21] while the Lennard-Jones parameters, A_{ii} and B_{ii}, for pure solute-solute and pure solvent-solvent interactions, are taken from Berendsen.[60] The combining rules

$$\varepsilon_{ij} = (\varepsilon_{ii}\,\varepsilon_{jj})^{1/2}\,, \tag{A30}$$

and

$$\sigma_{ij} = \frac{1}{2}\,(\sigma_{ii} + \sigma_{jj})\,, \tag{A31}$$

in which $A_{ii} = 4\varepsilon_{ii}\sigma_{ii}^{12}$ and $B_{ii} = 4\varepsilon_{ii}\sigma_{ii}^{6}$, are used to compute the Lennard-Jones parameters for solute-solvent interactions. For convenience in our calculations, we define σ_{HH} for hydrogen atom interactions to be equal to σ_{OO} for oxygen atom interactions (There is no well defined parameter for H-H and this definition is used for consistency in the combining rules.). Using the above combining rules, there is a relationship between a_i, b_i and the Lennard-Jones parameters for pure atom-atom interactions as follows:

If i = O,H then

$$a_i = 2\varepsilon_{ii}^{1/2}\sigma_{OO}^{12}\,,$$
$$b_i = 2\varepsilon_{ii}^{1/2}\sigma_{OO}^{6}\,. \tag{A32}$$

If i = Cl, CH_3 then

$$a_i = 2\varepsilon_{ii}^{1/2}\frac{1}{\sigma_{OO}^{6}}\left[\frac{\sigma_{OO}+\sigma_{ii}}{2}\right]^{12},$$
$$b_i = 2\varepsilon_{ii}^{1/2}\frac{1}{\sigma_{OO}^{3}}\left[\frac{\sigma_{OO}+\sigma_{ii}}{2}\right]^{6}. \tag{A33}$$

The parameters, γ_i^a and γ_i^b are given in Table A1. To focus on the influence of the switching charges on the dynamics, the constants α_i^a, β_i^a, α_i^b and β_i^b, given in Table A1, are set equal to zero to turn off the variation of the Lennard-Jones parameters with reaction progress.

Finally, for the solvent atoms, the forces due to the presence of the other solvent molecules and the solute atoms are

$$\mathbf{F}_j^{NB} = \sum_{i=A}^{C} \Gamma_{ji}\mathbf{r}_{ji} - \frac{\partial V^{Water}}{\partial \mathbf{r}_j}$$

$$= \Gamma_{jA}\mathbf{r}_{jA} + \Gamma_{jB}\mathbf{r}_{jB} + \Gamma_{jC}\mathbf{r}_{jC} - \frac{\partial V^{Water}}{\partial \mathbf{r}_j} . \tag{A34}$$

Table A1

	q_i /(kcal Å/mol)$^{1/2}$			a_i /(kcal Å^{12}/mol)$^{1/2}$			b_i /(kcal Å^6/mol)$^{1/2}$		
i	α_i^q	β_i^q	γ_i^q	α_i^a	β_i^a	γ_i^a	α_i^b	β_i^b	γ_i^b
A	-4.3688	1.1255	-11.3645	0.0	0.0	6008.2526	0.0	0.0	62.6221
B	0.0000	-2.2510	4.5020	0.0	0.0	2623.0416	0.0	0.0	47.1798
C	4.3688	1.1255	-11.3645	0.0	0.0	6008.2526	0.0	0.0	62.6221
O	0.0000	0.0000	-12.00666	0.0	0.0	793.322	0.0	0.0	25.0128
H	0.0000	0.0000	6.00333	0.0	0.0	1.245	0.0	0.0	0.03935

APPENDIX B

The switching function, $\sigma(z)$, satisfies the following criteria:

$$\begin{array}{lll} \text{for} \quad z \le 0 & \sigma(z) = 1 & \sigma'(z) = 0 \\ \text{for} \ 0 < z < z_0 & 0 < \sigma(z) < 1 & \sigma'(z) < 0 \\ \text{for} \quad z \ge z_0 & \sigma(z) = 0 & \sigma'(z) = 0 \end{array} . \tag{B1}$$

The functional form of $\sigma(z)$ in our calculations is

$$\sigma(z) = \begin{cases} 1 & z \le 0 \\ 1 - (z/z_0)^3(10 - (z/z_0)(15 - 6(z/z_0))) & 0 < z < z_0 \\ 0 & z > z_0 \end{cases} . \tag{B2}$$

Denoting Cl by A, CH_3 by B, and Cl′ by C, and letting $\rho = (r_{AB}^2 - r_{BC}^2)$, and κ be an adjustable positive constant, the image points of the complex are

$$\mathbf{r}_1 = [1-\sigma(\kappa\rho)]\mathbf{r}_A + \sigma(\kappa\rho)\mathbf{r}_B \tag{B3}$$

and

$$\mathbf{r}_2 = \sigma(-\kappa\rho)\mathbf{r}_B + [1-\sigma(-\kappa\rho)]\mathbf{r}_C . \tag{B4}$$

For $\rho >> 0$ we have $A^- + BC$, for $\rho \approx 0$ we have $[A{-}{-}B{-}{-}C]^-$, and for $\rho << 0$ we have $AB + C^-$. Thus we have a smooth transition of grouping along the reaction coordinate, minimizing the effects of our finite system size.

For the case where $\rho > 0$, the modification to the solute-solvent potential is as follows:
Define

$$\mathbf{r}_\alpha \equiv \text{image point of group } \alpha = \begin{cases} \mathbf{r}_1 & \alpha = A \\ \mathbf{r}_2 & \alpha = BC \end{cases} , \tag{B5}$$

$$\mathbf{r}_\beta \equiv \text{image point of solvent molecule } \beta = \text{position of oxygen atom} , \tag{B6}$$

$$\mathbf{r}_{\alpha\beta} = \mathbf{r}_\alpha - \mathbf{r}_\beta , \tag{B7}$$

$$s^2 \equiv \text{square of switching region minimum value} , \tag{B8}$$

$$V_{ij} \equiv \text{Lennard-Jones Coulomb potential between solute atom } i \text{ and solvent atom } j . \tag{B9}$$

The potential energy of interaction between solute atom i and solvent atom j, where atom j is a member

of solvent molecule β, is

$$U_{ij} = \sigma(r_{\alpha\beta}^2 - s^2)V_{ij} \,. \tag{B10}$$

The same type of analysis applies when $\rho < 0$. For the solvent-solvent interactions, the interaction potential between two atoms, i and j, from different solvent molecules, β_1 and β_2, is

$$U_{ij} = \sigma(r_{\beta_1\beta_2}^2 - s^2)\, V_{ij} \,. \tag{B11}$$

For our system of 64 waters, $z_0 = 11.0$ Å^2, $s = 5.94$ Å, and $\kappa = 0.9$.

References

1. A. J. Parker, Chem. Rev. **69**, 1 (1969).
2. W. M. Olmstead and J. I. Brauman, J. Am. Chem. Soc. **99**, 4219 (1977).
3. D. K. Bohme and G. I. Mackay, J. Am. Chem. Soc. **103**, 978 (1981).
4. W. J. Albery and M. M. Kreevoy, Adv. Phys. Org. Chem. **16**, 87 (1978).
5. C. K. Ingold, *Structure and Mechanism in Organic Chemistry* (2nd Ed., Cornell University Press, Ithaca, N. Y., 1969).
6. T. H. Lowry and K. S. Richardson, *Mechanism and Theory in Organic Chemistry* (2nd Ed., Harper and Row, New York, 1981).
7. C. Reichardt, *Solvent Effects in Organic Chemistry* (Verlag Chemie, Weinheim, New York, 1979).
8. J. Chandrasekhar, S. F. Smith, and W. L. Jorgensen, J. Am. Chem. Soc. **106**, 3049 (1984).
9. J. Chandrasekhar, S. F. Smith, and W. L. Jorgensen, J. Am. Chem. Soc. **107**, 154 (1985).
10. R. A. Chiles and P. J. Rossky, J. Am. Chem. Soc. **106**, 6867 (1984).
11. G. van der Zwan and J. T. Hynes, J. Chem. Phys. **76**, 2993 (1982).
12. G. van der Zwan and J. T. Hynes, J. Chem. Phys. **78**, 4174 (1983).
13. G. van der Zwan and J. T. Hynes, Chem. Phys. **90**, 21 (1984).
14. J. P. Bergsma, P. M. Edelsten, B. J. Gertner, K. R. Huber, J. R. Reimers, K. R. Wilson, S. M. Wu, and J. T. Hynes, Chem. Phys. Lett. **123**, 394 (1986).
15. J. P. Bergsma, J. R. Reimers, K. R. Wilson, and J. T. Hynes, J. Chem. Phys. (submitted, 1986).
16. M. J. Pellerite and J. I. Brauman, J. Am. Chem. Soc. **105**, 2672 (1983).
17. A. Dedieu and A. Veillard, J. Am. Chem. Soc. **94**, 6730 (1972).
18. A. Dedieu and A. Veillard, in *Quantum Theory of Chemical Reactions, Vol. 1*, edited by R. Daudel, A. Pullman, L. Salem and A. Veillard (Reidel, Dordrecht, 1979) p. 69.
19. S. Wolfe, D. J. Mitchell, and H. B. Schegel, J. Am. Chem. Soc. **103**, 7692 (1981).
20. K. Morokuma, J. Am. Chem. Soc. **104**, 3732 (1982).
21. R. O. Watts, Chem. Phys. **26**, 367 (1977).
22. B. J. Gertner, J. P. Bergsma, K. R. Wilson, S. Lee, and J. T. Hynes, J. Chem. Phys. (submitted, 1986).
23. D. J. Adams, in *The Problem of Long-Range Forces in the Computer Simulation of Condensed Media*, edited by D. Ceperly (National Resource for Computation in Chemistry, Berkeley, 1980) p. 13.
24. W. C. Swope, H. C. Andersen, P. H. Berens, and K. R. Wilson, J. Chem. Phys. **76**, 637 (1982).
25. D. Beeman, J. Comput. Phys. **20**, 130 (1976).
26. R. W. Hockney and J. W. Eastwood, *Computer Simulation Using Particles* (McGraw-Hill Inc., New York, N. Y., 1981).
27. P. J. Kuntz, in *Dynamics of Molecular Collisions, Part B*, edited by W. H. Miller (Plenum Press, New York, N. Y., 1976) p. 53.

28. G. Herzberg, *Molecular Spectra and Molecular Structure III. Electronic Spectra and Electronic Structure of Polyatomic Molecules* (Van Nostrand Reinhold, New York, N. Y., 1967).
29. S. Glasstone, K. J. Laidler, and H. Eyring, *Theory of Rate Processes* (McGraw-Hill, New York, 1941).
30. K. Kuchitsu and Y. Morino, Bull. Chem. Soc. Japan 38, 814 (1965).
31. P. H. Berens, D. H. J. Mackay, G. M. White, and K. R. Wilson, J. Chem. Phys. 79, 2375 (1983).
32. G. M. White and K. R. Wilson, J. Chem. Phys. (submitted, 1985).
33. J. P. M. Postma , Ph.D. thesis, University of Groningen, 1985.
34. K. Heinzinger and P. C. Vogel, Z. Naturforsch 29, 1164 (1974).
35. P. C. Vogel and K. Heinzinger, Z. Naturforsch 30, 789 (1975).
36. J. C. Keck, Discuss. Faraday Soc. 33, 173 (1962).
37. J. B. Anderson, J. Chem. Phys. 58, 4684 (1973).
38. C. H. Bennett, in *Algorithms for Chemical Computations: ACS Symposium Series 46*, edited by R. E. Christofferson (American Chemical Society, Washington, D. C., 1977) p. 63.
39. C. H. Bennett, in *Diffusion in Solids*, edited by J. J. Burton (Academic Press, New York, 1975) p. 73.
40. R. O. Rosenberg, B. J. Berne, and D. Chandler, Chem. Phys. Lett. 75, 162 (1980).
41. J. A. McCammon, Rpts. Prog. Phys. 47, 1 (1984).
42. M. Karplus and J. A. McCammon, CRC Crit. Rev. Biochem. 9, 293 (1981).
43. J. A. McCammon and M. Karplus, Accts. Chem. Rev. 16, 1 (1983).
44. E. K. Grimmelman, J. C. Tully, and E. Helfand, J. Chem. Phys. 74, 5300 (1981).
45. J. J. Grabowski, J. M. van Doren, V. M. Bierbaum, and C. H. DePuy , (private communication).
46. E. Wigner, Trans. Faraday Soc. 34, 29 (1938).
47. J. P. Valleau and G. M. Torrie, J. Comput. Phys. 23, 187 (1977).
48. D. H. J. Mackay, P. M. Edelsten, and K. R. Wilson , (to be submitted).
49. S. H. Northrup and J. T. Hynes, J. Chem. Phys. 73, 2700 (1980).
50. R. F. Grote and J. T. Hynes, J. Chem. Phys. 73, 2715 (1980).
51. R. F. Grote and J. T. Hynes, J. Chem. Phys. 75, 2191 (1981).
52. G. E. Walrafen, in *Water, A Comprehensive Treatise, Vol. 1, The Physics and Chemistry of Water*, edited by F. Franks (Plenum, New York, 1972) p. 151.
53. H. A. Kramers, Physica (The Hague) 7, 284 (1940).
54. R. F. Grote, G. van der Zwan, and J. T. Hynes, J. Phys. Chem. 88, 4676 (1984).
55. J. A. Rice , University of California, San Diego, Dept. of Mathematics (to be published).
56. D. J. McLennan, Aust. J. Chem. 31, 1897 (1978).
57. R. H. Bathgate and E. A. Moelwyn-Hughes, J. Chem. Soc., 26421 (1959).
58. S. S. Shaik, Prog. Phys. Org. Chem. 16, 197 (1985).
59. A. Pross, Adv. Phys. Org. Chem. 21, 99 (1985).
60. J. C. Berendsen, Proc. Natl. Acad. Sci. 80, 4315 (1983).

Figure Captions

Figure 1. Gas phase potential energy LEPS surface contour plot as a function of the AB and BC bond lengths, r_1 and r_2, for a linear arrangement of $[Cl—CH_3—Cl]^-$, a barrier height of 13.9 kcal/mol with respect to the bottom of the wells, and a barrier frequency of $\omega_b = 461$ cm^{-1}. The contour values are in kcal/mol units, and the zero in potential is for separated species $Cl^- + CH_3Cl$.

Figure 2. Variation of charge on the three atoms of the reaction system as a function of $r_{AB}^2 - r_{BC}^2$, in which the charge is given in units of the charge of an electron. Note that the charge variation on the central united atom, CH_3, shows a slight dip (*i.e.* becomes less positive) in charge near the transition barrier. This is different than the slight increase in positive charge which would be obtained if one simply summed the charges on the atoms of CH_3 to a single point charge, as is discussed in Appendix A and shown in Fig. 15.

Figure 3. Plot of the average internal energy redistribution of $[Cl—CH_3—Cl]^-$, versus time for the reaction $Cl^- + CH_3Cl \rightarrow ClCH_3 + Cl^-$ on the 13.9 kcal/mol energy barrier surface for an ensemble of 128 trajectories in the gas phase. Time zero is when the reaction system is first released at the saddle point. The barrier height for the linear configuration, relative to separated species, is approximately 3.6 kcal/mol. The total energy is partitioned into $[Cl—CH_3—Cl]^-$ potential energy, $[Cl—CH_3—Cl]^-$ potential energy plus $CH_3—Cl$ vibrational kinetic energy, $CH_3—Cl$ rotational and translational kinetic energy, and the translational kinetic energy of the Cl^- ion. The vibrational kinetic energy plus total $[Cl—CH_3—Cl]^-$ potential energy increases to a maximum in about 0.25 ps before and after the transition barrier but decreases at longer times. This build up in energy and subsequent decrease is observed on a shorter time scale for the translational and rotational degrees of freedom. The kinetic energy at longer times is seen to transform into potential energy, and a metastable complex is formed. In the gas phase, in contrast to the solution trajectories described later, the total $[Cl—CH_3—Cl]^-$ potential plus kinetic energy is conserved.

Figure 4. Schematic diagram showing a typical thermodynamic free energy profile along the reaction coordinate for a S_N2 reaction, $X^- + RY \rightarrow XR + Y^-$, in the gas phase (solid line) and in a polar solvent (dashed line). The standard free energy picture is that the polar solvent will stabilize the higher charge density reactants and products more than the lower charge density transition state complex. The energy wells in the gas phase are characteristic of a metastable charge dipole complex which can form close to the transition barrier, and will mostly disappear in solution (in thermodynamic free energy terms).

Figure 5. Schematic illustration of some predominant recrossing patterns observed in the molecular dynamics simulation of A + BC reaction dynamics on low barriers in solution. The dividing line represents the transition barrier dividing surface between reactants on the left and products on the right, while the arrows indicate the direction of the trajectories: (a) is a direct, successful reactant → product (RP) transition with no recrossing (Only this type of trajectory occurs in the TST picture.); (b) is a single recrossing, reactant → product → reactant (RR), after the transition barrier is crossed in the forward direction, and (c) is a single recrossing, product → reactant → product (PP), in which the recrossing occurs prior to an initial reactant → product crossing.

Figure 6. Solvent time dependent friction on the reaction coordinate for a linear geometry of $[Cl—CH_3—Cl]^-$ at the transition barrier as function of time, normalized by the value of the friction at

time zero. The magnitude of the friction at time zero is ω_ζ^2, with $\omega_\zeta = 890\ cm^{-1}$. When the time dependent friction is computed for a typical bent geometry of $[Cl—CH_3—Cl]^-$ at the transition barrier, the result is the same as for the linear geometry.

Figure 7. Variation of charge on the three atoms of the reaction system as a function of $r_{AB}^2 - r_{BC}^2$, in which the charge is given in units of the charge of an electron. Here, the charge migration along the reaction coordinate is made to pass through an inflection point at the transition barrier, thus giving a partial charge configuration which is the same at the transition barrier as in Fig. 2 but which has a zero first derivative with respect to the reaction coordinate at the transition barrier.

Figure 8. Illustration of the coulombic bias at the transition barrier for ensembles of each of the three reaction outcomes described in Fig. 5. The average electric potential (*cf* Eq 3.7) at the "left-hand" chloride atom, Cl, is compared to that for the "right-hand" chloride atom, Cl′, as a function of the radius of a sphere of neighboring atoms included in the calculation of the potential. In addition, the average electric potential is computed for the sum of all three ensembles, *i.e.* for an ensemble of essentially all trajectories. Reactants are defined as $Cl + CH_3Cl'$ and products are defined as $ClCH_3 + Cl'$. The figure shows that there is a greater electric potential at the "left-hand" chloride atom, Cl, for reactions crossing the transition barrier twice from reactants to reactants (RR), and a larger potential at the "right-hand" chloride atom, Cl′, for those reactions which cross the transition barrier twice from products to products (PP), but no obvious difference in electric potential for the reactions which cross once from reactants to products (RP), nor for the sum of all trajectories.

Figure 9. Schematic representation of the effect of the frozen solvent linear and quadratic potentials when added to the gas phase potential energy profile along the reaction coordinate. The frozen solvent potentials shift the location of the equilibrium transition barrier forward or backward along the reaction coordinate and to higher energy. Note that the peak of the gas phase potential is lowered to $V_T(0)$, which includes equilibrium solvation.

Figure 10. Rotational time correlation functions, P_1 and P_2, for the H-O-H angle bisector for 87 molecules of liquid water. These correlation functions are defined as $\langle P_n [\hat{\mathbf{d}}\cdot\hat{\mathbf{d}}(t)] \rangle$, where P_n is the n'th Legendre polynomial, and $\hat{\mathbf{d}}(t)$ is the unit vector along the angle bisector (approximately along the dipole moment vector) at time t. Note the similarity between these correlation functions and the time dependent friction for water acting on the reaction coordinate as shown in Fig. 6.

Figure 11. Outcomes of 1000 trajectories on the 13.9 kcal/mol barrier and normal charge switching (*cf* Fig. 2), plotting initial kinetic energy along the asymmetric stretch reaction coordinate versus the relative shift in energy, ΔV, from the gas phase transition barrier. The symbol '+' represents trajectories which cross the transition barrier once from reactants to products (RP), circles, 'O', represent trajectories which begin as reactants and cross the transition barrier twice to end up as reactants (RR), while triangles ,'Δ', are trajectories which begin as products and cross the transition barrier twice to reform products (PP). The lines of slope 1 and -1 represent the threshold of kinetic energy required to overcome the additional potential energy, ΔV, to give a successful reaction.

Figure 12. Plot of the average energy partitioning of $[Cl—CH_3—Cl]^-$ versus time for the reaction $Cl^- + CH_3Cl \rightarrow ClCH_3 + Cl^-$ on the 13.9 kcal/mol energy barrier for an ensemble of 100 trajectories in water solvent. Time zero is when the reaction system is first released at the saddle point. The total reaction system energy is partitioned into $[Cl—CH_3—Cl]^-$ potential energy plus $CH_3—Cl$ vibrational kinetic energy, $CH_3—Cl$ rotational kinetic energy, and the translational kinetic energies of the $CH_3—Cl$

and of the Cl^- ion. Note that the increase in total reaction system energy shortly before and after the transition barrier is largely due to an increase in the kinetic energy of vibration, Note that the vibrational energy of CH_3—Cl decays rapidly to solvent on a subpicosecond time scale.

Figure 13. Solvent time dependent friction on the reaction coordinate as a function of time, normalized by the value of the friction at time zero, for a heavy mass water system in which the mass of hydrogens is replaced by the mass of oxygen, but all other variables remain unchanged. The magnitude of the friction at time zero is the same as for the H_2O solvent system ($\omega_\zeta = 890\ cm^{-1}$), but the initial short time decay in the correlation is slower than that for pure water which is shown in Fig. 6. It is interesting to note that the longer time behavior is nearly the same as in Fig. 6.

Figure 14. Outcome of 500 trajectories on the 13.9 kcal/mol barrier with a 1/8'th charge switching rate. Initial kinetic energy along the asymmetric stretch reaction coordinate is plotted versus the relative shift in energy, ΔV, from the gas phase transition barrier. For details, see Fig. 11.

Figure 15. Collapsed charge version of variation of charge on the three atoms of the reaction system as a function of $r_{AB}^2 - r_{BC}^2$, in which the charge is given in units of the charge of an electron. The slight increase in positive charge for the CH_3 group is obtained by summing the charges on the atoms of CH_3 to a single point charge, as is discussed in Sec. IV and in Appendix A.

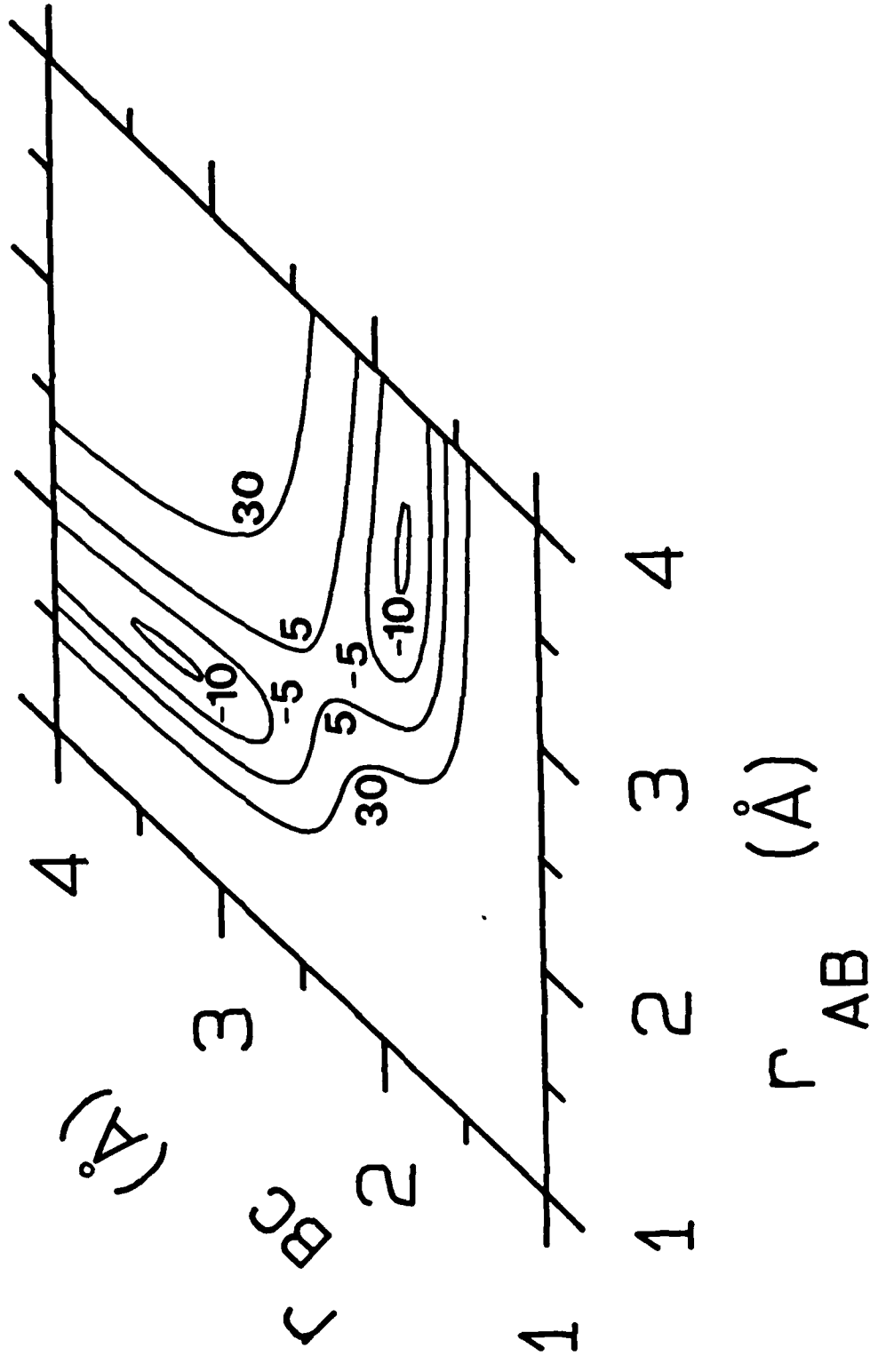

FIGURE 1

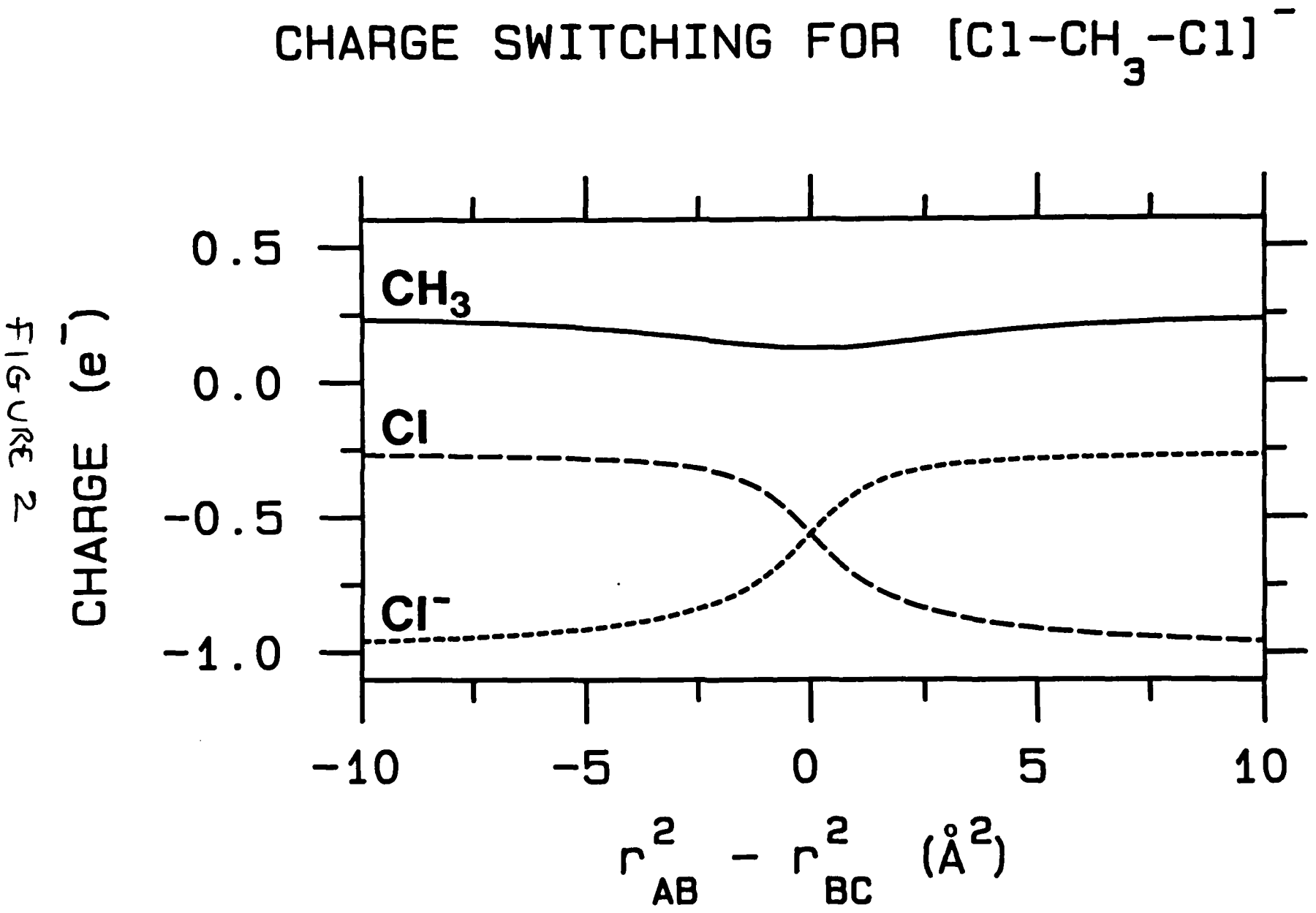
CHARGE SWITCHING FOR [Cl-CH3-Cl]-
CHARGE (e-)
0.5
0.0
-0.5
-1.0
CH3
Cl
Cl-
-10
-5
0
5
10
r2AB - r2BC (Å2)

FIGURE 2

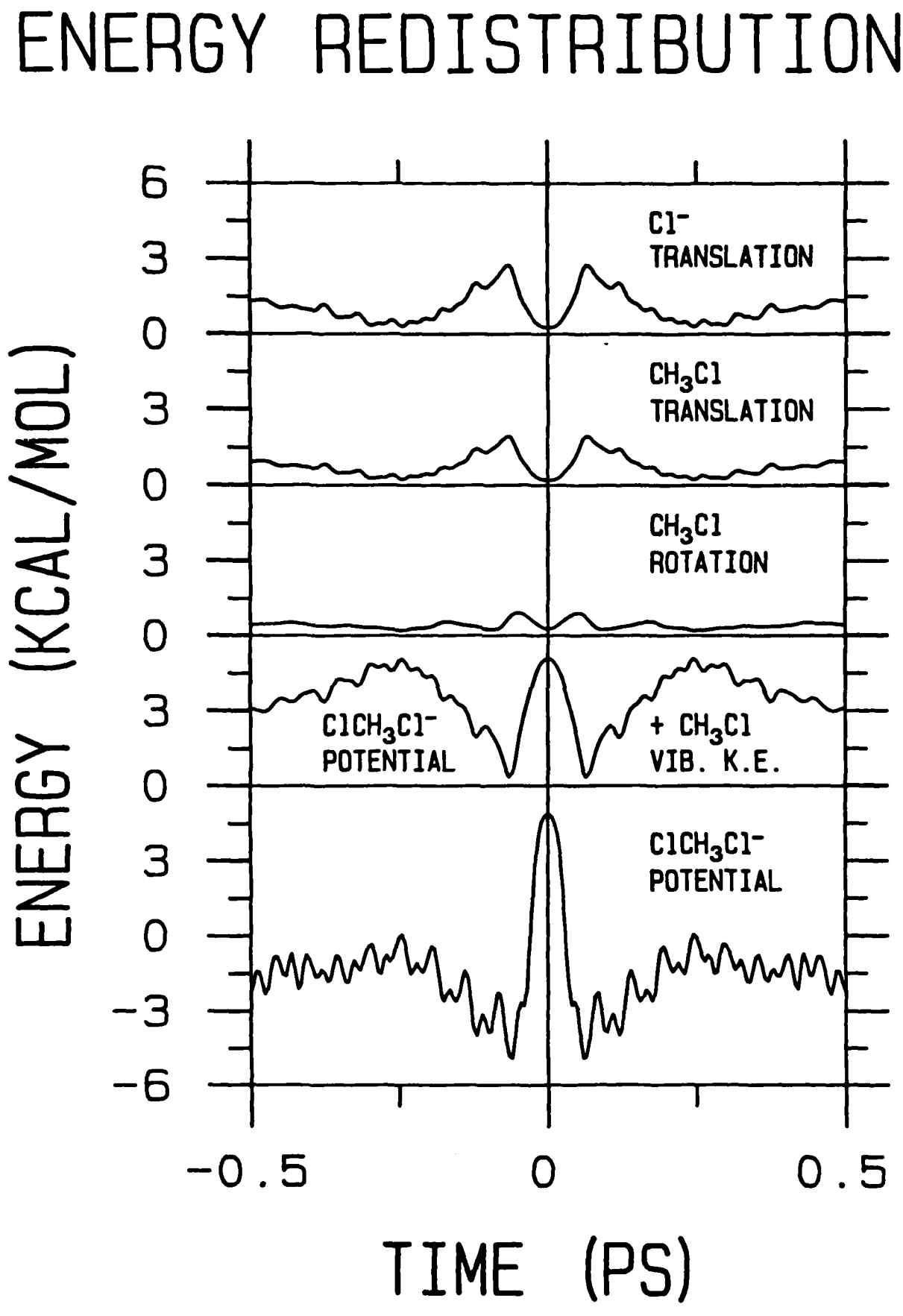
ENERGY REDISTRIBUTION
ENERGY (KCAL/MOL)
6
3
0
3
0
3
0
3
0
3
0
-3
-6
Cl⁻ TRANSLATION
CH3Cl TRANSLATION
CH3Cl ROTATION
ClCH3Cl⁻ POTENTIAL
+ CH3Cl VIB. K.E.
ClCH3Cl⁻ POTENTIAL
-0.5
0
0.5
TIME (PS)

FIGURE 3

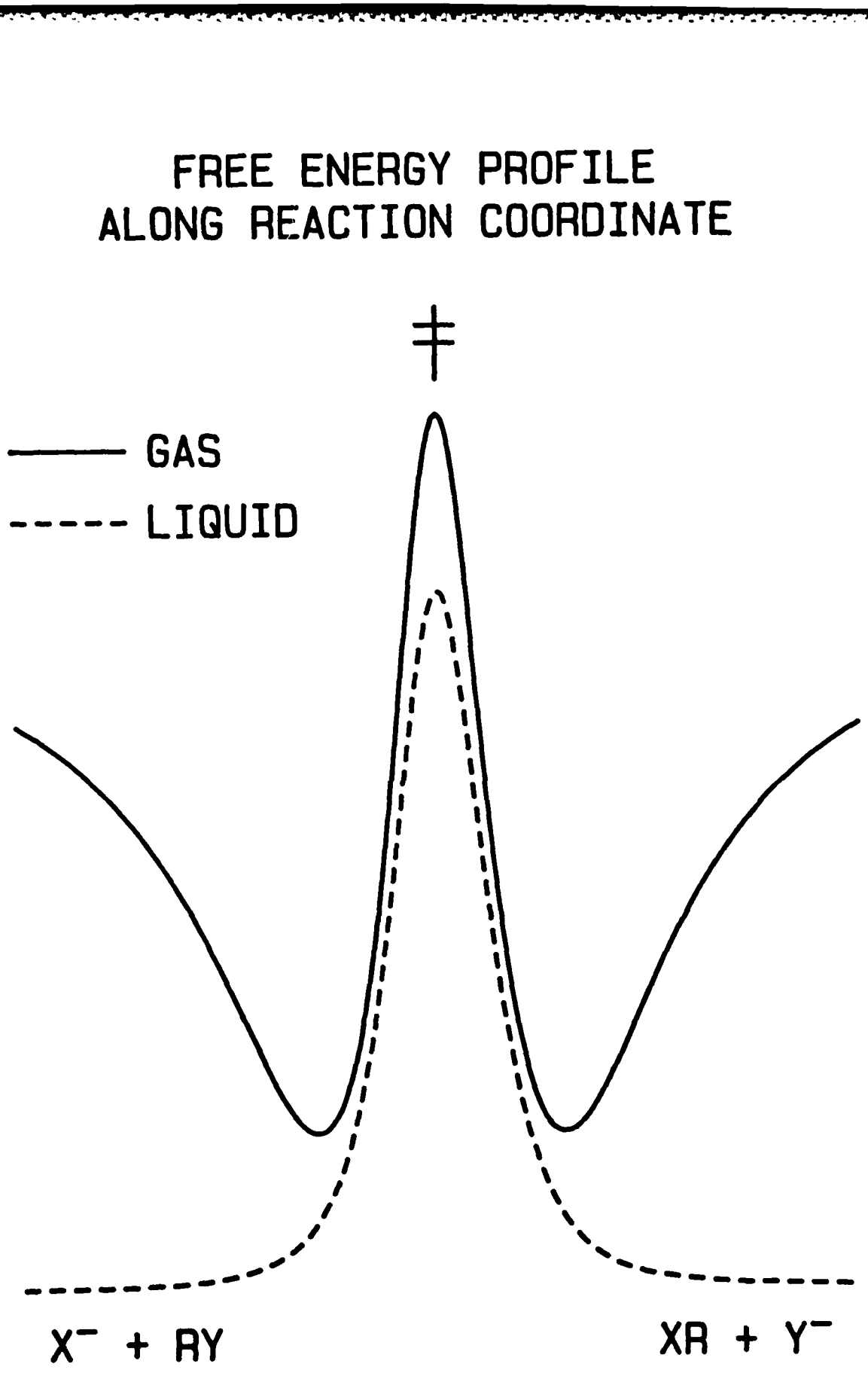
FREE ENERGY PROFILE
ALONG REACTION COORDINATE
‡
GAS
LIQUID
X⁻ + RY
XR + Y⁻

FIGURE 4

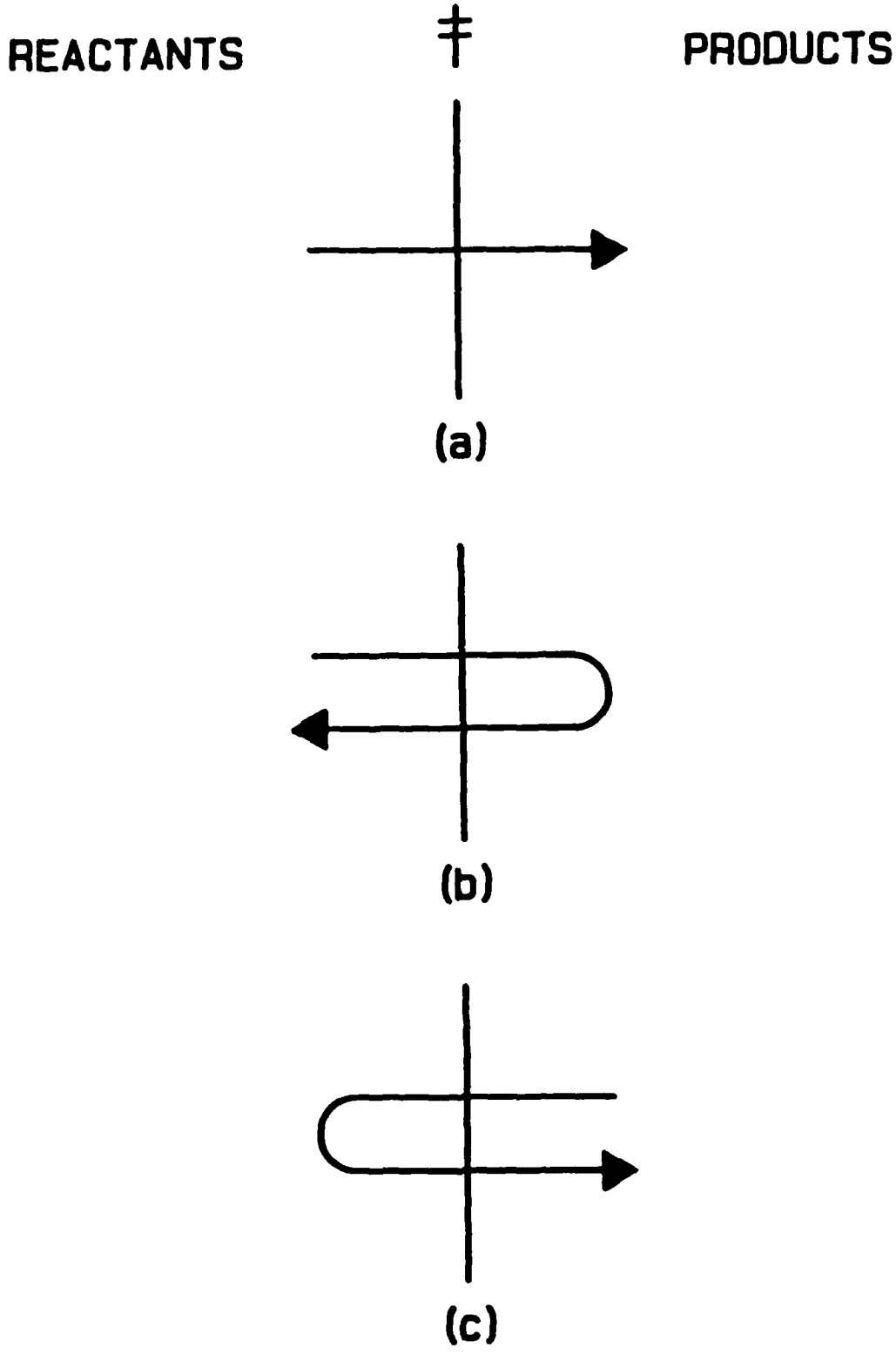

FIGURE 5

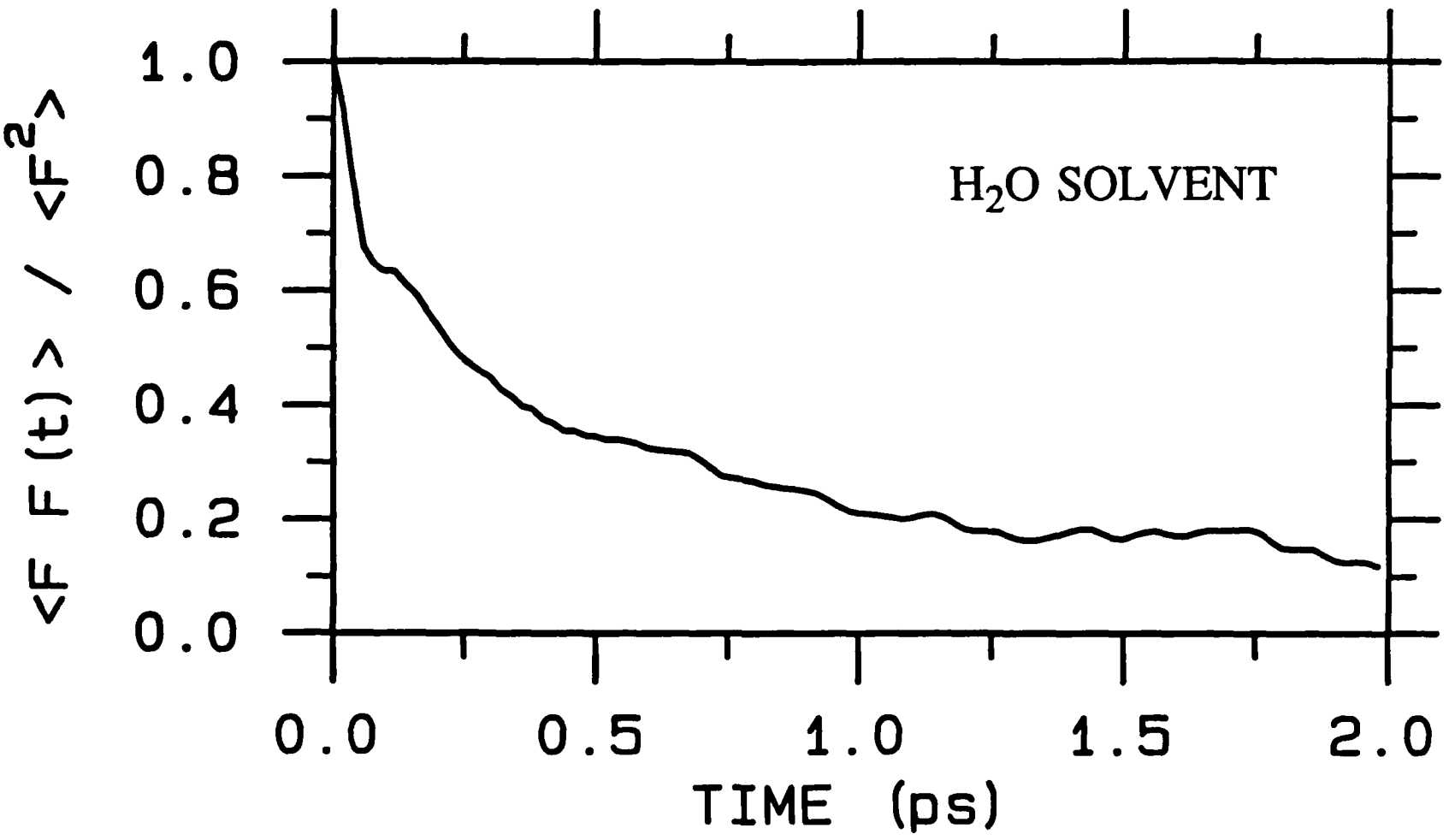
TIME DEPENDENT FRICTION
H_2O SOLVENT
<F F(t)> / <F²>
1.0
0.8
0.6
0.4
0.2
0.0
0.0
0.5
1.0
1.5
2.0
TIME (ps)

FIGURE 6

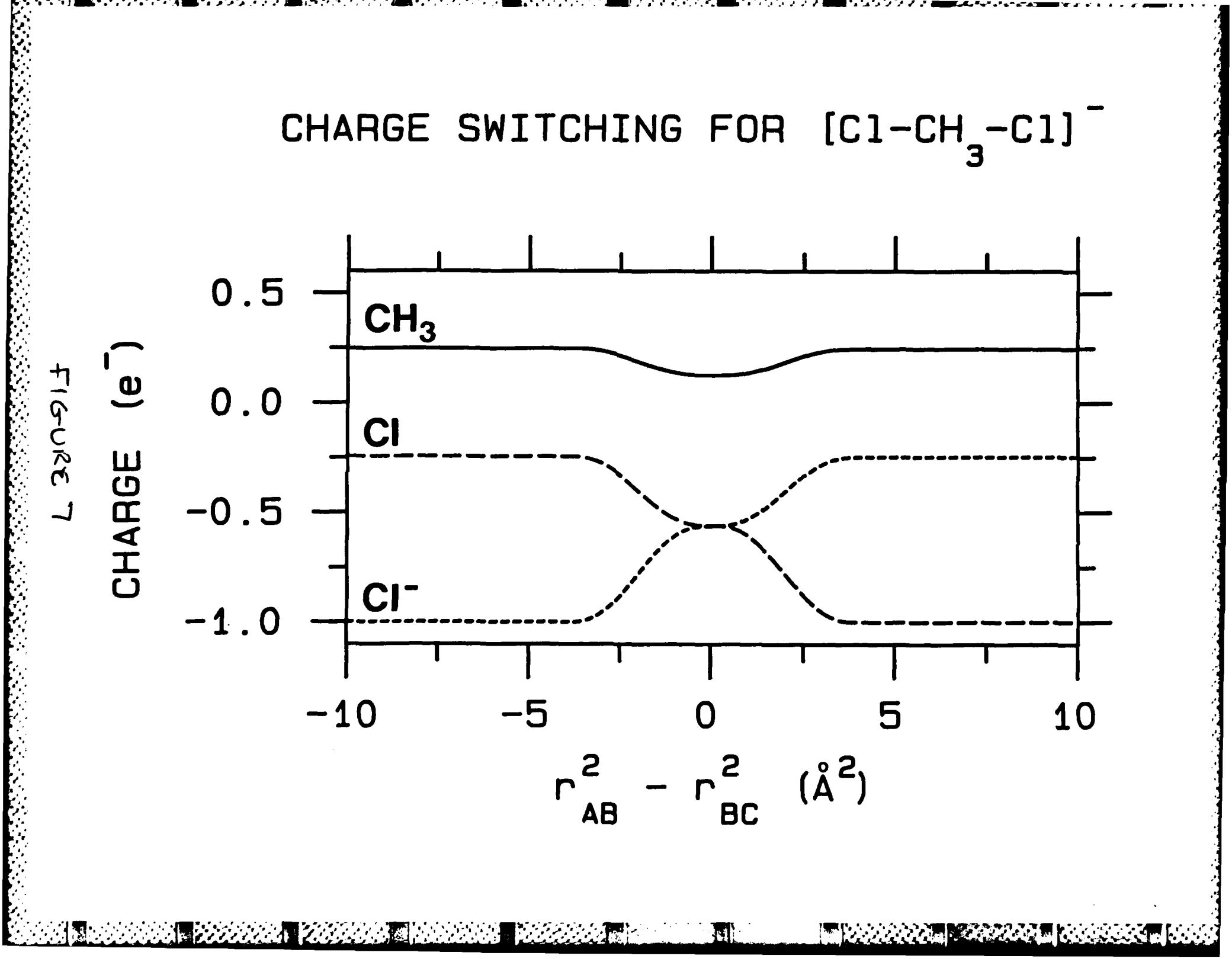
CHARGE SWITCHING FOR [Cl-CH3-Cl]-
CHARGE (e-)
0.5
0.0
-0.5
-1.0
CH3
Cl
Cl-
-10
-5
0
5
10
r2AB - r2BC (Å2)

FIGURE 7

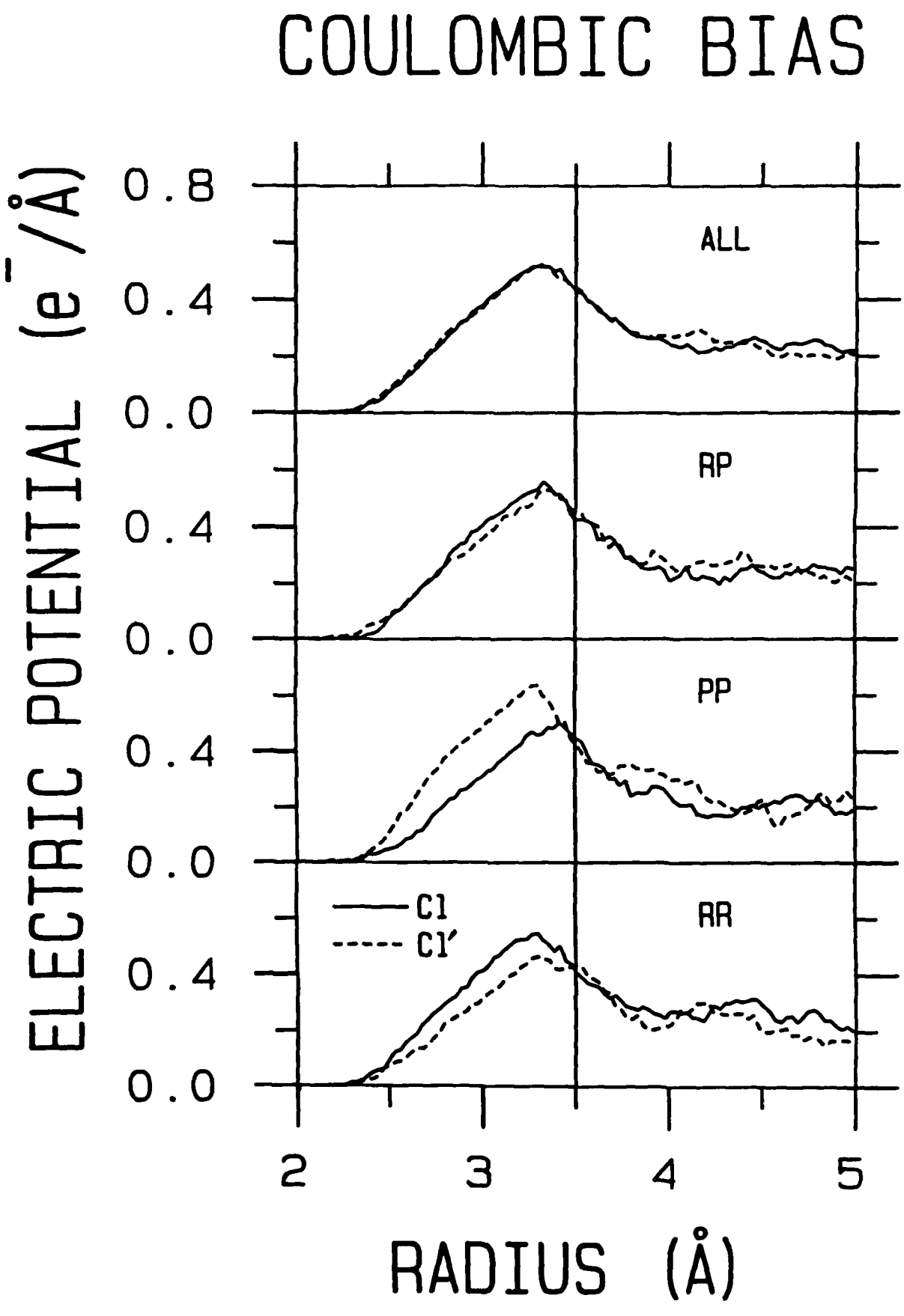
COULOMBIC BIAS
ELECTRIC POTENTIAL (e⁻/Å)
0.8
0.4
0.0
ALL
RP
PP
RR
C1
C1'
2
3
4
5
RADIUS (Å)

FIGURE 8

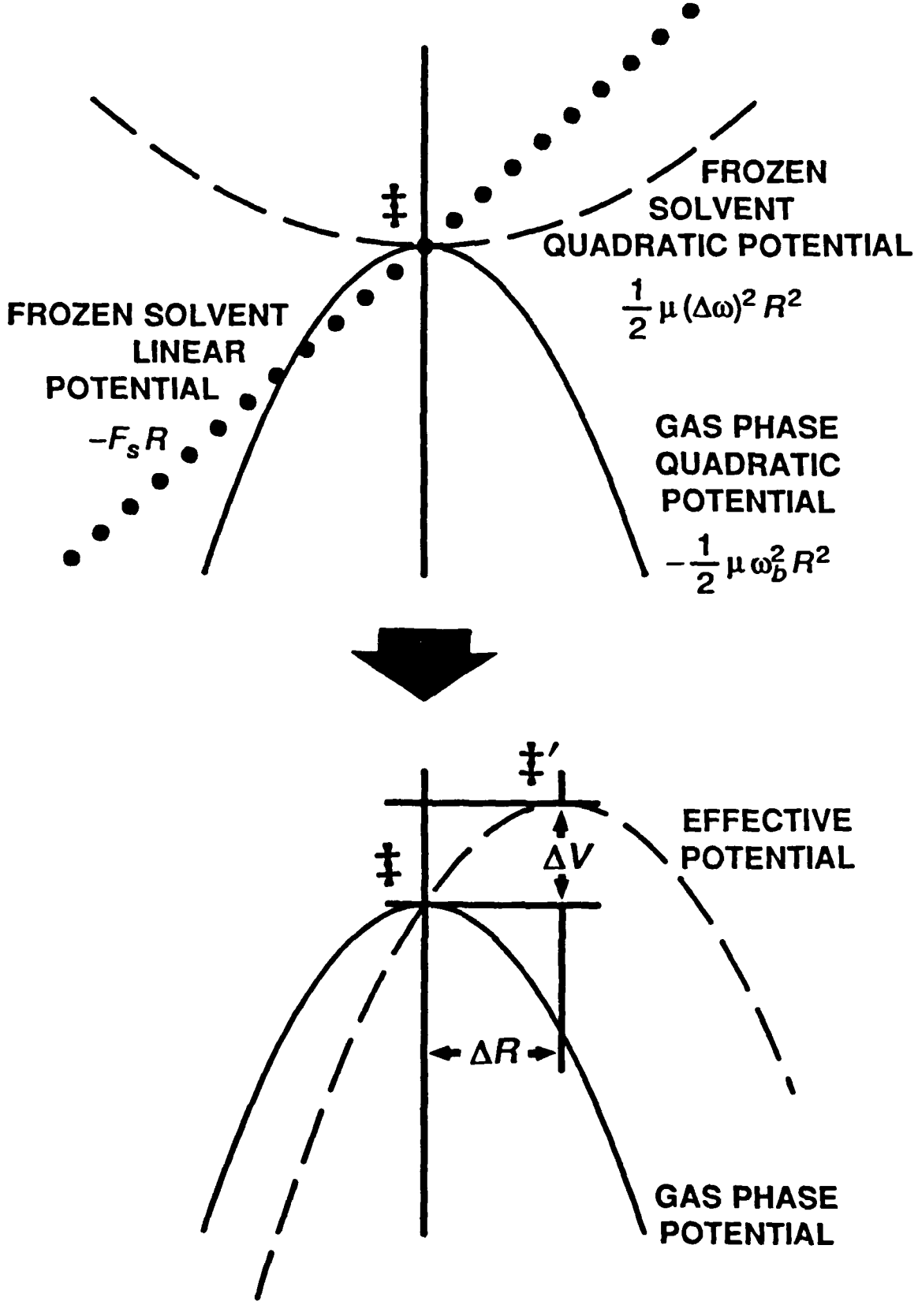
FROZEN SOLVENT QUADRATIC POTENTIAL
$\frac{1}{2}\mu(\Delta\omega)^2 R^2$
FROZEN SOLVENT LINEAR POTENTIAL
$-F_s R$
GAS PHASE QUADRATIC POTENTIAL
$-\frac{1}{2}\mu\omega_b^2 R^2$
‡
‡′
EFFECTIVE POTENTIAL
ΔV
ΔR
GAS PHASE POTENTIAL

FIGURE 9

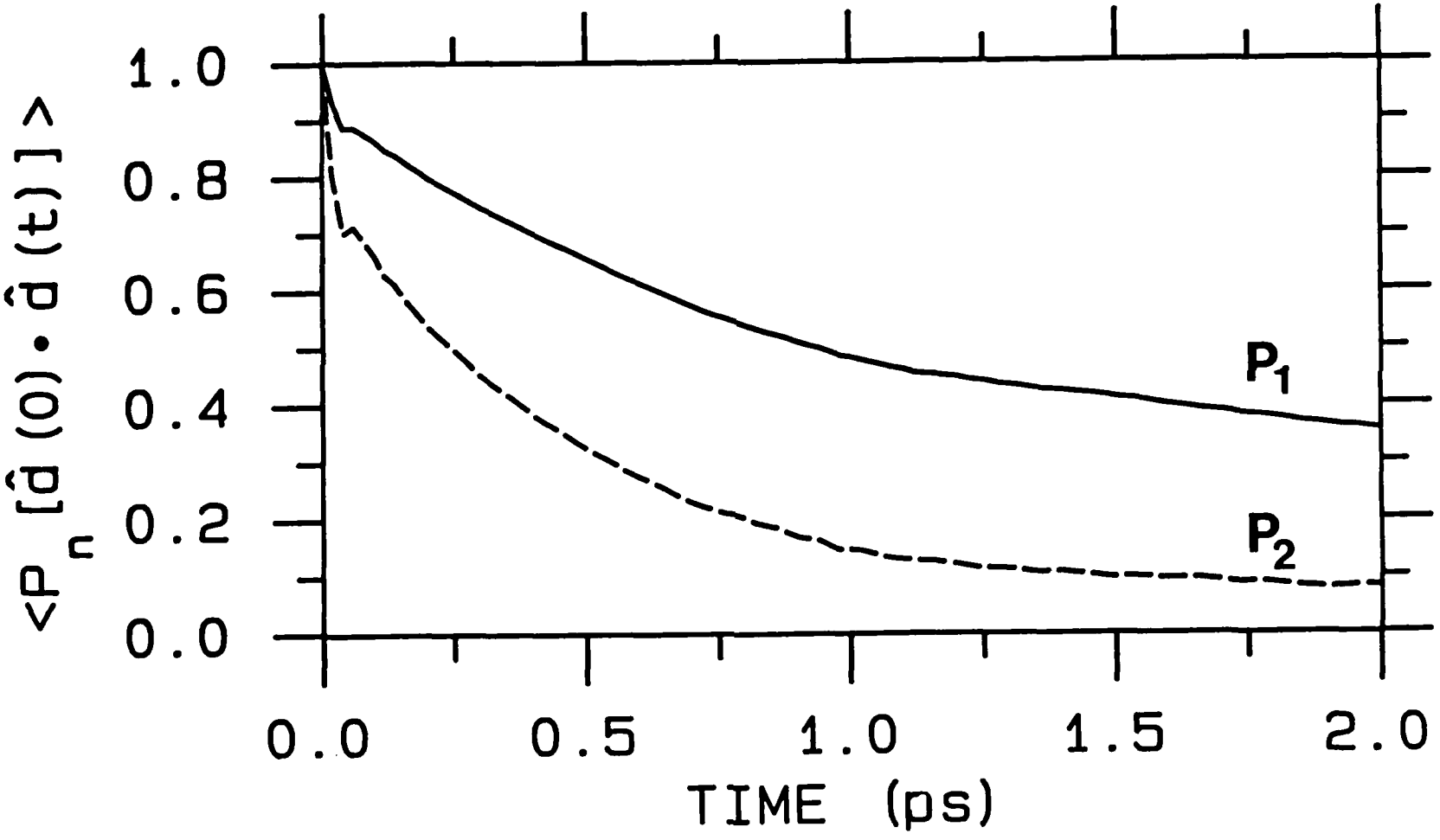
ROTATIONAL CORRELATION FOR H_2O
$\langle P_n [\hat{d}(0) \cdot \hat{d}(t)] \rangle$
1.0
0.8
0.6
0.4
0.2
0.0
P_1
P_2
0.0
0.5
1.0
1.5
2.0
TIME (ps)

FIGURE 10

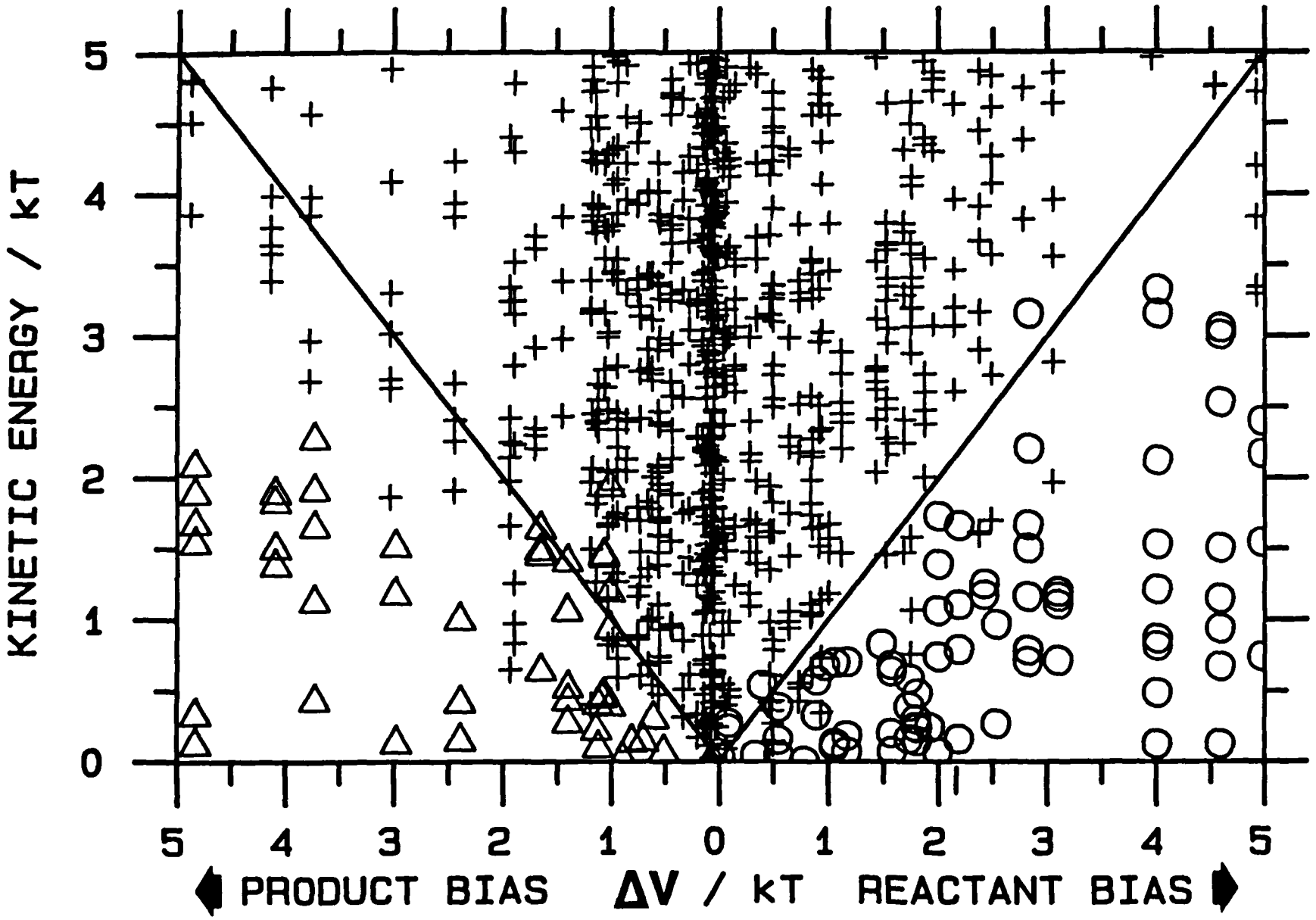
KINETIC ENERGY / kT
0
1
2
3
4
5
5 4 3 2 1 0 1 2 3 4 5
PRODUCT BIAS ΔV / kT REACTANT BIAS

FIGURE 11

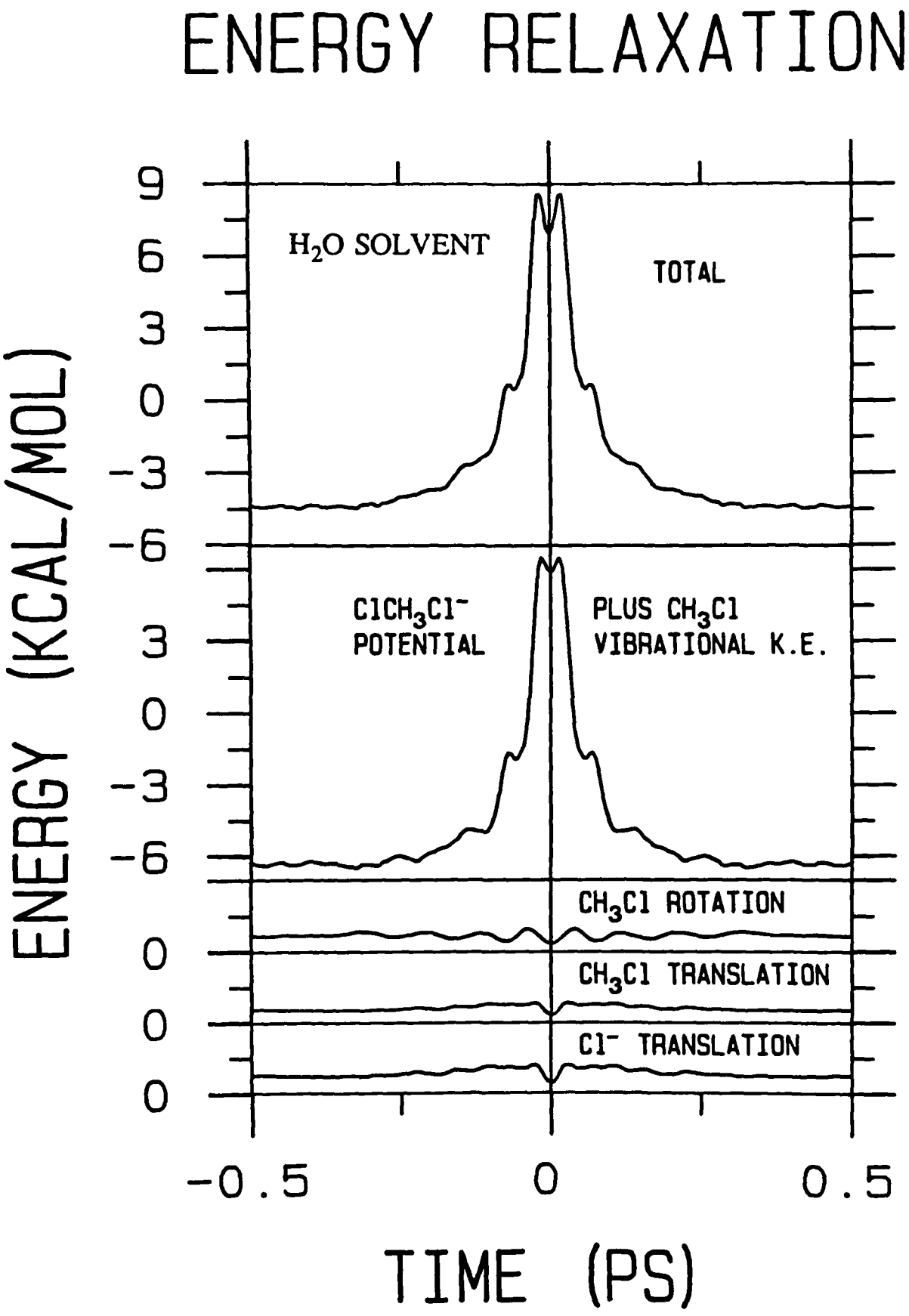
ENERGY RELAXATION
H_2O SOLVENT
TOTAL
$ClCH_3Cl^-$ POTENTIAL
PLUS CH_3Cl VIBRATIONAL K.E.
CH_3Cl ROTATION
CH_3Cl TRANSLATION
Cl^- TRANSLATION
ENERGY (KCAL/MOL)
9
6
3
0
-3
-6
3
0
-3
-6
0
0
0
-0.5
0
0.5
TIME (PS)

FIGURE 12

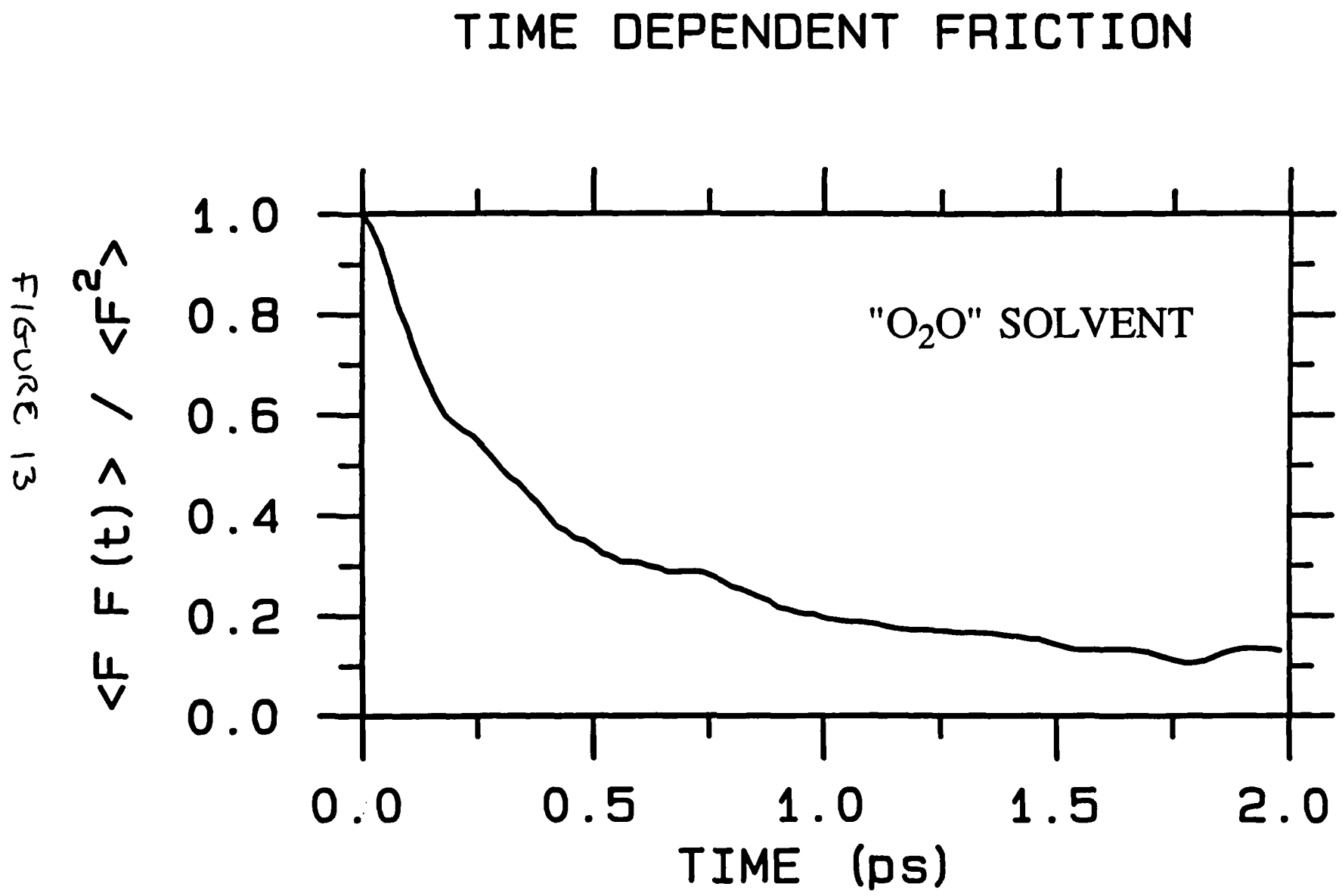
TIME DEPENDENT FRICTION
"O_2O" SOLVENT
$\langle F\,F(t)\rangle / \langle F^2\rangle$
1.0
0.8
0.6
0.4
0.2
0.0
0.0
0.5
1.0
1.5
2.0
TIME (ps)

FIGURE 13

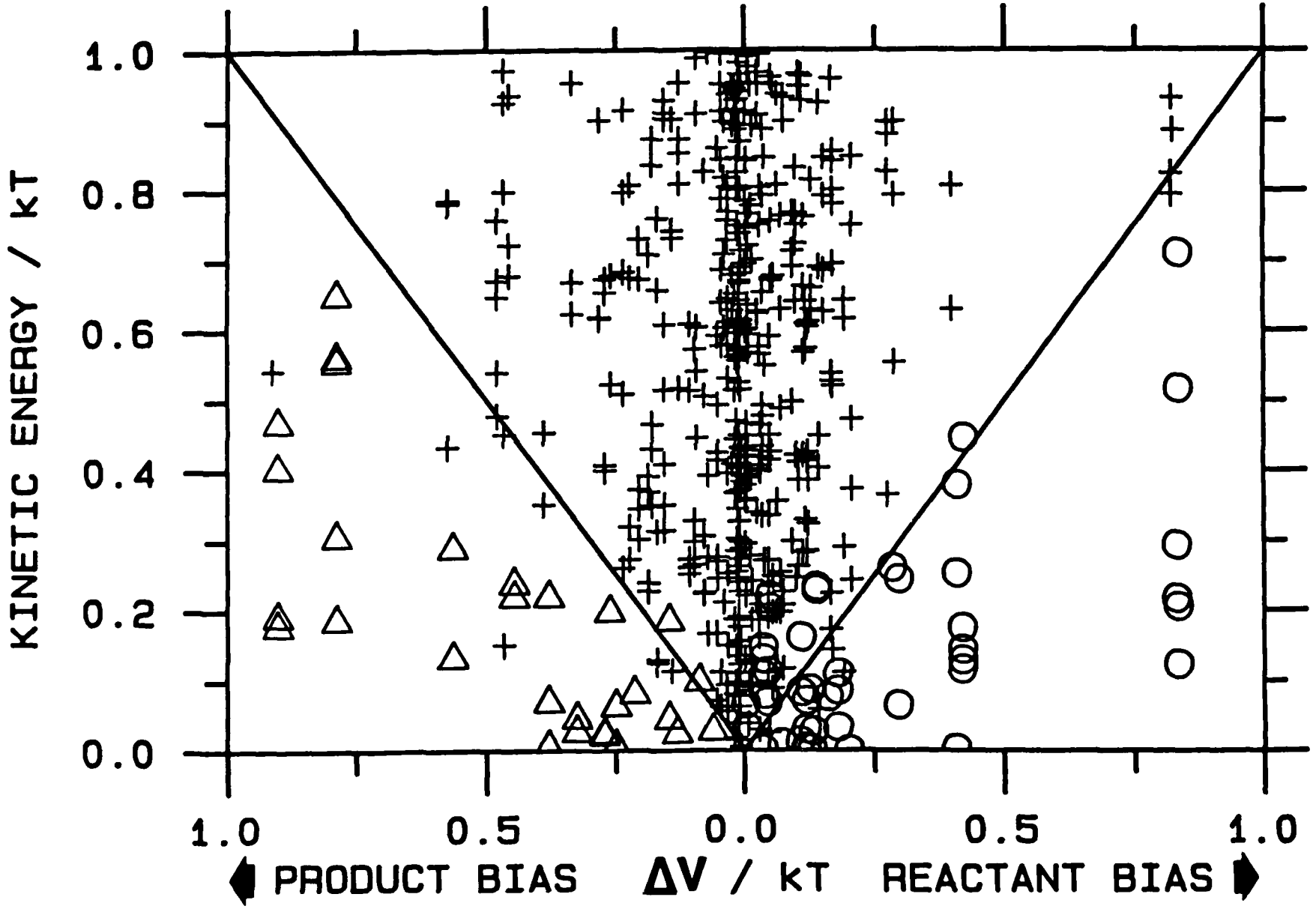
KINETIC ENERGY / kT
1.0
0.8
0.6
0.4
0.2
0.0
1.0
0.5
0.0
0.5
1.0
PRODUCT BIAS
ΔV / kT
REACTANT BIAS

FIGURE 14

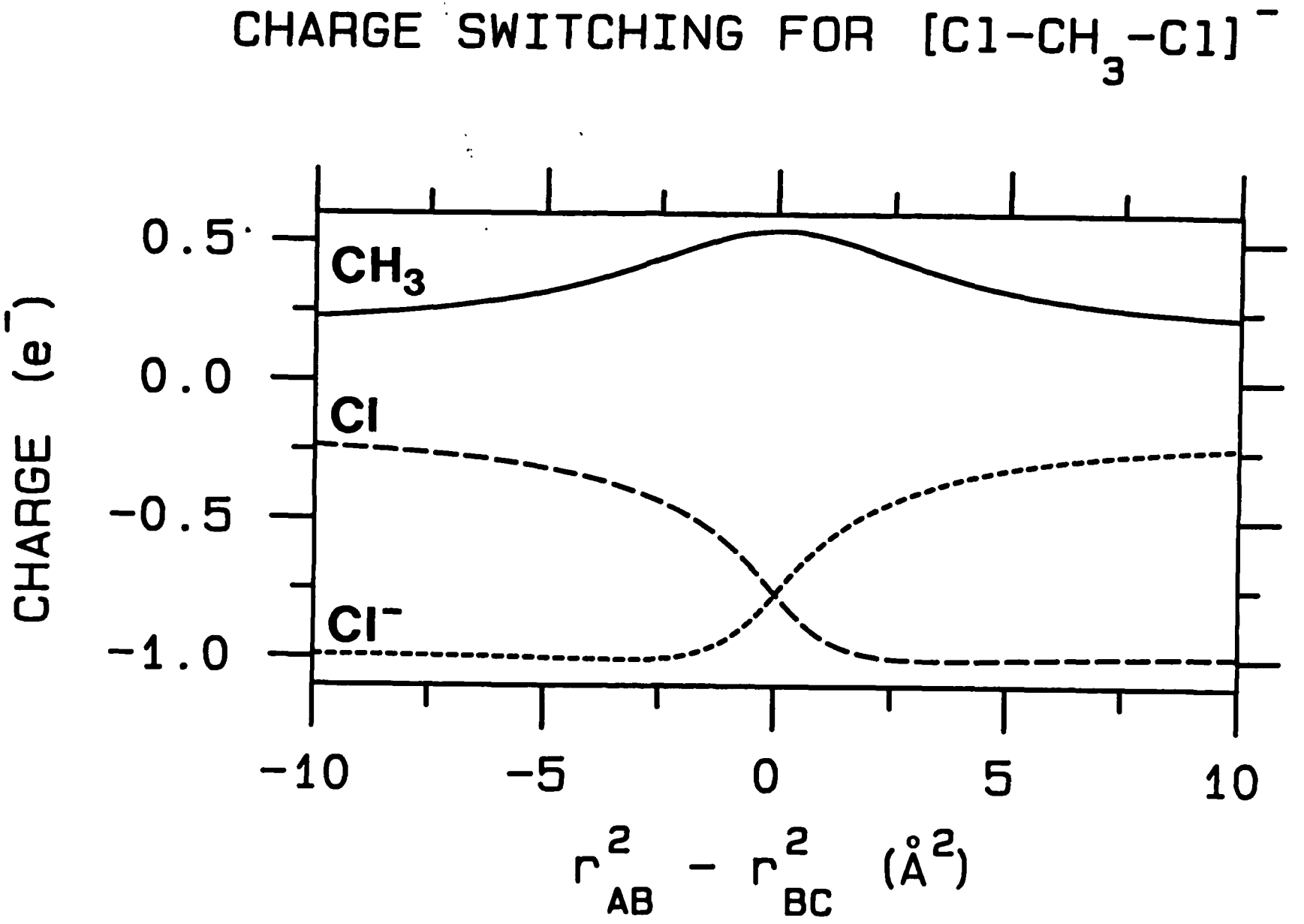
CHARGE SWITCHING FOR [Cl-CH3-Cl]-
0.5
0.0
-0.5
-1.0
CH3
Cl
Cl-
CHARGE (e-)
-10
-5
0
5
10
r2AB - r2BC (Å2)

FIGURE 15

END

DTIC

6-86